ACS SyntheticBiology

pubs.acs.org/synthbio

Research Article

Programming Probiotics: Diet-Responsive Gene Expression and Colonization Control in Engineered *S. boulardii*

Deniz Durmusoglu,[§] Daniel J. Haller,[§] Ibrahim S. Al'Abri,[§] Katie Day, Carmen Sands, Andrew Clark, Adriana San-Miguel, Ruben Vazquez-Uribe, Morten O. A. Sommer, and Nathan C. Crook*

Cite This: *ACS Synth. Biol.* 2024, 13, 1851−1865

Read Online

ACCESS | Metrics & More | Article Recommendations | Supporting Information

ABSTRACT: *Saccharomyces boulardii* (*Sb*) is an emerging probiotic chassis for delivering biomolecules to the mammalian gut, offering unique advantages as the only eukaryotic probiotic. However, precise control over gene expression and gut residence time in *Sb* have remained challenging. To address this, we developed five ligand-responsive gene expression systems and repaired galactose metabolism in *Sb*, enabling inducible gene expression in this strain. Engineering these systems allowed us to construct AND logic gates, control the surface display of proteins, and turn on protein production in the mouse gut in response to dietary sugar. Additionally, repairing galactose metabolism expanded *Sb*'s habitat within the intestines and resulted in galactose-responsive control over gut residence time. This work opens new avenues for precise dosing of therapeutics by *Sb* via control over its *in vivo* gene expression levels and localization within the gastrointestinal tract.

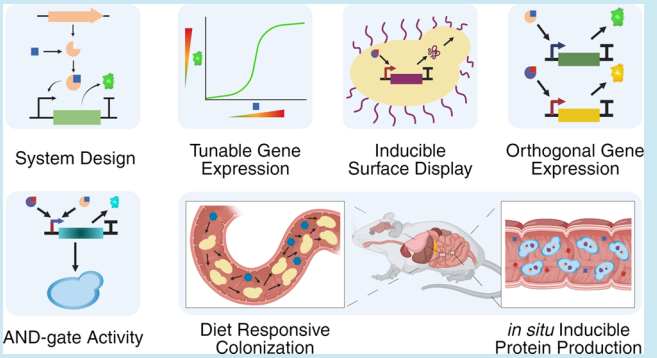

KEYWORDS: *synthetic biology, yeast, microbiome*

INTRODUCTION

Engineered probiotics are microorganisms that are genetically engineered to deliver biotherapeutics, detect disease biomarkers, or perform other beneficial functions in the gut environment, therefore providing unique advantages for disease prevention and treatment.[1] Specifically, engineered probiotics can convert nutrients available in the gut to molecules that are not, or cannot be readily biosynthesized by the host.[1] Additionally, probiotics can be engineered to eliminate undesirable molecules, such as antinutrients or toxins. Recently, bacterial probiotics have been engineered to target pathogens such as *Clostridioides difficile* or *Pseudomonas aeruginosa*, treat metabolic diseases such as phenylketonuria, and deliver biotherapeutics such as interleukin-10 to treat inflammatory bowel disease.[2−4] Furthermore, engineered probiotics can sense and respond to their environment, improving targeting and dosage of therapeutics.[5] For example, probiotic strains of *Escherichia coli* were recently engineered to detect tetrathionate and thiosulfate, markers of inflammation, in the murine gut, demonstrating how engineered probiotics can be programmed to respond to conditions in the gut.[6,7] Engineered probiotics can therefore potentially be used as a drug delivery platform for current therapies or enable new treatments for unmet needs in the gut environment. While all engineered probiotics that are currently in clinical trials are bacterial probiotics, engineered yeast probiotics have seen growing preclinical interest due to their high rates of protein secretion, stability under lyophilization, and ability to function during antibiotic treatment.[8−13]

Saccharomyces boulardii (*S. boulardii* or *Sb*) is a probiotic yeast that was first isolated from lychee and mangosteen by Henri Boulard in 1923.[14,15] Compared to *Saccharomyces cerevisiae* (with which it shares 99% genomic relatedness),[16] *Sb* can better tolerate low pH and human body temperature, enabling improved survival in the human gut.[17−19] *Sb* is currently used to treat ulcerative colitis, diarrhea, and recurrent *Clostridium difficile* infection.[20−24] Wild-type *Sb* is generally recognized as safe (GRAS) and persists in conventionally raised mice for up to 24 h, antibiotic-treated mice for up to 10 days, and in humans for approximately one week.[25−27] Recently, a suite of genetic engineering tools for *Sb* have been developed, including transformation methods, constitutive promoters, genome editing protocols, genomic integration sites, G protein-coupled receptors, and secretion-enhancing gene knockouts.[26,28−30]

The overall activity of a probiotic-delivered function is the product of the per-cell gene expression level and the abundance

Received: February 28, 2024
Revised: May 6, 2024
Accepted: May 10, 2024
Published: May 24, 2024

https://doi.org/10.1021/acssynbio.4c00145
ACS Synth. Biol. 2024, 13, 1851−1865

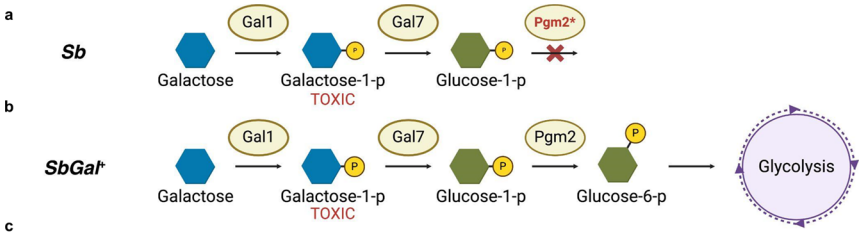

c

		Single C Source					Double C Source					
Carbon Source	Glucose	2%	-	-	-	-	2%	1%	0.5%	2%	1%	0.5%
	Galactose	-	2%	-	-	-	2%	1%	2%	-	-	-
	Lactose	-	-	2%	-	-	-	-	-	-	-	-
	Xylose	-	-	-	2%	-	-	-	-	-	-	-
	Raffinose	-	-	-	-	2%	-	-	-	2%	1%	2%
OD600	*Sb*	1.28	0.02	0.19	0.16	0.8	1.32	1.14	1.12	0.02	0.02	0.04
	SbGal+	1.16	1.28	0.16	0.12	0.78	1.33	1.24	1.13	1.23	1.09	0.87

Figure 1. Repair of *PGM2* enables metabolism of galactose by *S. boulardii* (a) Diagram illustrating the galactose utilization pathway in *Sb*, with an inactive *PGM2* enzyme leading to toxic intermediate accumulation. (b) Engineered *SbGal*$^+$ pathway, showing the restoration of *PGM2* activity, allowing for efficient galactose metabolism. (c) Growth comparison in complete synthetic media (CSM) with various carbon sources for wild-type *Sb* MYA-796 and the genetically repaired *Sb* MYA-796 (*SbGal*$^+$). The data illustrates the improved growth of *SbGal*$^+$ on 2% galactose, demonstrating the benefits of *PGM2* repair (orange highlighting). Minimal to no growth difference between *Sb* and *SbGal*$^+$ was observed on alternative sugars like xylose and lactose, which do not utilize the galactose metabolic pathway. *SbGal*$^+$ enhanced growth when raffinose is present with glucose, suggesting the strain's potential for improved performance in complex sugar environments, such as the gut. Values represent the averages of end point optical densities of three biological replicates grown in the indicated media for 36 h.

of the probiotic at the target site. A major challenge in the development of engineered probiotics is control over these two properties. If the expression of a therapeutic is constitutive, i.e. "always on", then cessation of treatment becomes dependent on probiotic washout, which can be variable between individuals.[5] Additionally, biosynthesis of a therapeutic is often energy- and nutrient-intensive, decreasing the fitness of the engineered probiotic and reducing its abundance in the gut.[31] To date, all in vivo applications of *Sb* have used constitutive expression systems. Therefore, it would be advantageous to control the timing and dosage of the delivered therapeutic in *Sb*. To enable such control in other organisms, ligand-responsive gene expression systems are often employed.[32,33] Ligand-responsive gene expression systems can activate or deactivate transcription of a specific gene in the presence of a particular inducer molecule.[34] For *Sb*, this molecule could be provided through the patient's diet/medication (if in vivo expression is desired) or directly to the culture medium (if expression during production is desired). The level of gene expression is thus regulated by the concentration of inducer molecule provided, enabling custom dosage of a therapeutic. Ligand-responsive expression systems also enable construction of more complex circuits, such as logical AND and OR gates, enabling more control over the behavior of engineered probiotics.[35,36] Additionally, ligand-responsive expression systems can improve the biosafety of the therapeutic, as human-to-human spread of the engineered probiotic does not result in drug delivery of the therapeutic to unintended individuals.[37,38]

In this work, we sought to investigate the performance in *Sb* of ligand-responsive gene expression systems that were previously investigated in *S. cerevisiae* and demonstrate their utility for several in vivo applications. We first constructed *SbGal*$^+$, a galactose-competent strain of *Sb*, and demonstrated its improved growth relative to wild-type on galactose and other sugars. We next investigated the dose−response behavior in *SbGal*$^+$ of five inducible promoters that respond to galactose, xylose, lactose or IPTG (isopropyl ß-D-1-thiogalactopyranoside), copper, and anhydrotetracycline, respectively, and span a variety of gene activation ranges under both aerobic and anaerobic (i.e., gut-like) conditions. Several of these inducible systems are regulated by nontoxic (e.g., galactose, IPTG, xylose) or minimally toxic (e.g., aTc at the tested concentrations) small molecules. We then demonstrated the applicability of this inducible promoter set for applications such as yeast surface display and logic gate construction. When delivered to the mouse gut, we showed that the *SbGal*$^+$ strain exhibits improved colonization when galactose is added, likely due to galactose's dual role as a carbon source. Finally, we constructed a logical AND gate using these inducible promoters and demonstrated programmable control of gene expression in probiotic yeast during passage through the mouse gut. This research therefore unveils enhanced, precision-controlled *Sb* expression systems, which will find utility in advancing personalized disease intervention strategies.

RESULTS AND DISCUSSION

Repair of *S. boulardii* PGM2 Gene Enables Growth on Galactose and Raffinose. We first chose to investigate the galactose-inducible promoter *pGAL1* for our toolkit of inducible systems in *Sb*. *pGAL1* is one of the most commonly used promoters for inducible gene expression in *S. cerevisiae* due to its extensive characterization and high dynamic range.[39] Also, as one of the monosaccharides comprising the lactose disaccharide, it is generally nontoxic to humans, except in the case of galactosemia, a rare genetic disorder that prevents galactose metabolism.[40] Liu et al. demonstrated that the *PGM2* gene in *Sb* MYA-796 harbors a point mutation that introduces a premature stop codon (Figure 1A), leading to a truncated phosphoglucomutase enzyme and a very slow growth rate of *Sb* on galactose.[41] Liu et al. also demonstrated that when *Sb*'s *PGM2* gene is reverted to the sequence found in *S. cerevisiae*, growth on galactose is restored (Figure 1B). However, this study did not investigate the functionality of the *pGAL1* promoter in either wildtype *Sb* or in *Sb* with the *PGM2* gene repaired (henceforth *SbGal*$^+$).[41]

https://doi.org/10.1021/acssynbio.4c00145
ACS Synth. Biol. 2024, 13, 1851−1865

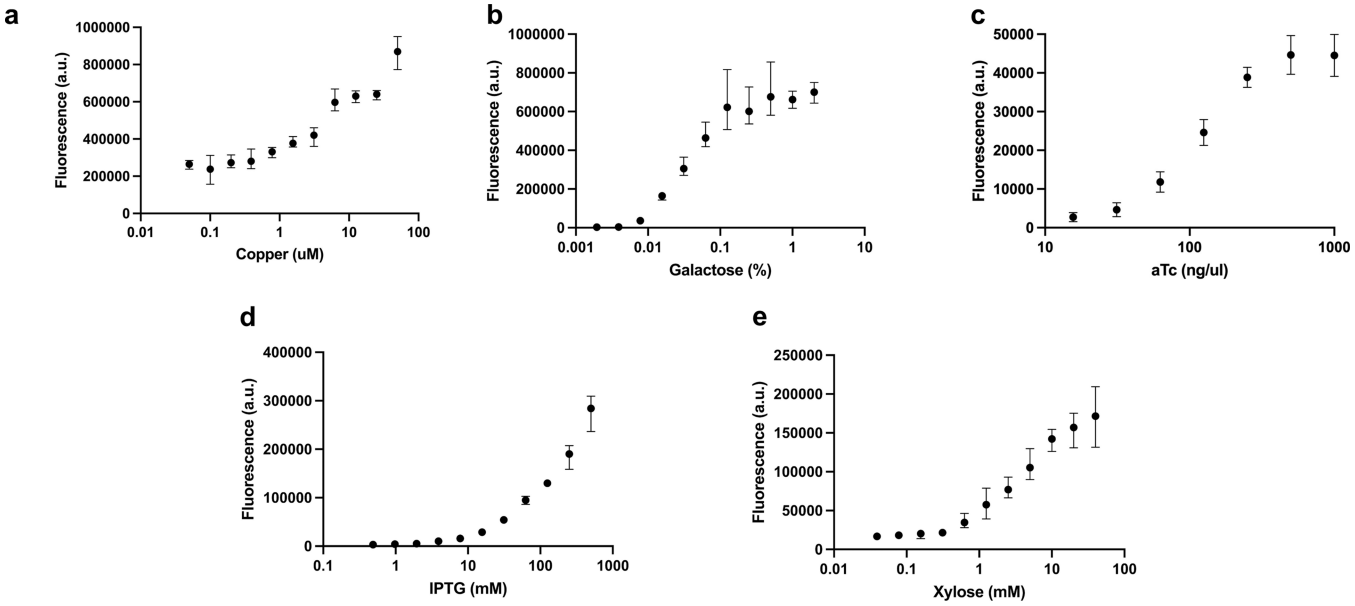

Figure 2. Inducible systems enable tunable gene expression in probiotic yeast. yeGFP was used to measure the activity of each promoter: *pCUP1* (a), *pGAL1* (b), *pTET* (c), *pLAC* (d), and *pXYL* (e) in response to different concentrations of galactose (a), copper (b), aTc (c), IPTG (d), and xylose (e). Inducible promoter-yeGFP constructs were placed on a high-copy (2 μ) plasmid with a *URA3* selective marker. For systems using heterologous repressors (tetR, lacI, and xylR), these repressors were expressed from a low-copy (CEN) plasmid with a *HIS3* marker. Strains containing the *pGAL1* construct were cultured at 37 °C in CSM media lacking uracil and supplemented with raffinose (2%) as a carbon source and exposed to various concentrations of galactose as an inducer. Strains containing the *pCUP1*, *pTET*, *pLAC*, and *pXYL* constructs were cultured at 37 °C in CSM media lacking either uracil or uracil and histidine supplemented with glucose (2%) with a range of copper, aTc, IPTG, and xylose concentrations, respectively. Three biological replicates were used for all measurements.

In order to enable cells to utilize galactose as both a nutrient source and as an inducer for gene expression, we first measured the growth of *Sb* and *SbGal*$^+$ on media containing a variety of carbon sources. As shown in Figure 1C, wildtype *Sb* grows very slowly at 37 °C on media with 2% galactose as the sole carbon source, while *SbGal*$^+$ grows at a much higher rate (Figures 1C and S1B,M), in agreement with Liu et al. Additionally, *SbGal*$^+$ appears to grow to a slightly lower optical density than wild-type *Sb* when grown on 2% glucose at 37 °C (Figures 1C and S1A). This is consistent with the hypothesis that the point mutation in *PGM2* enables better glucose utilization at 37 °C in *Sb*.[41] Notably, the growth advantage of *Sb* on glucose is eliminated at 30 °C (Figure S1L). Repair of the *PGM2* gene had minimal to no effect on the growth of *Sb* in media with xylose or lactose as the sole carbon source at 37 or 30 °C (Figures 1C and S1C,D,N,O). We also investigated the growth of *SbGal*$^+$ on raffinose, a trisaccharide containing units of galactose, glucose, and fructose. We found that *SbGal*$^+$ exhibits slightly improved growth relative to *Sb* at 37 °C with raffinose as the sole carbon source (Figures 1C and S1E) but similar growth as *Sb* at 30 °C (Figure S1P), possibly due to its improved ability to utilize the galactose monomer that may result from raffinose metabolism.

To further characterize the carbon metabolism of *SbGal*$^+$, we compared its growth in mixed carbon sources to that of *Sb*. We found no apparent differences in growth between the two strains when cultivated at 37 °C under media containing 2% glucose and 2% galactose (Figures 1C and S1F). When the concentration of glucose was more limited (1% glucose, 1% galactose), *Sb* and *SbGal*$^+$ exhibited similar growth for the first ∼18 h (Figure S1G). After this point, however, the growth rate of *Sb* slowed, likely due to the depletion of glucose in the media, while the growth rate of *SbGal*$^+$ remained high as it was able to switch to galactose metabolism after glucose depletion. This diauxic shift behavior indicates that glucose is the preferred carbon source for *SbGal*$^+$ (much like *S. cerevisiae*), but that *SbGal*$^+$ is capable of efficiently metabolizing galactose when glucose is scarce.[42] No difference between the two strains was observed at 37 °C when glucose was in excess of galactose (i.e., 2% glucose, 0.5% galactose, Figures 1C and S1H). When only raffinose and galactose are available as carbon sources, *Sb* grows extremely slowly at 37 °C, while *SbGal*$^+$ grows well (Figure S1I−K). The growth of *Sb* on mixed raffinose/galactose media improved at 30 °C, but the growth of *SbGal*$^+$ was still superior (Figure S1S,T). These results demonstrate that *SbGal*$^+$ is able to efficiently utilize galactose and raffinose as carbon sources, particularly at human body temperature.

Inducible Systems Enable Tunable Gene Expression in *S. boulardii*. Having confirmed expanded carbohydrate metabolism in *SbGal*$^+$, we next asked whether and to what extent gene expression could be induced by common small molecule inducers. For maximum compatibility with existing yeast toolkits, we used the galactose-inducible pG*AL1* promoter and the copper-inducible *pCUP1* promoter from the MoClo Yeast Toolkit (YTK),[43] as well as three engineered minimal promoters previously described: *pTET* (inducible by anhydrotetracycline (aTc)), *pLAC* (inducible by IPTG), and *pXYL* (inducible by xylose).[44] All three minimal promoters consist of two repressor-binding operator sequences, separated by spacers, placed upstream of a minimal *ADH2* transcriptional start site. To investigate the dose−response characteristics of these promoters in *SbGal*$^+$, we constructed plasmids encoding a yeast-enhanced green fluorescent protein (yeGFP) under the control of each of the inducible promoters and transformed these plasmids to *SbGal*$^+$. For those strains harboring the *pTET*, *pLAC*, and *pXYL* promoters, we also introduced plasmids encoding the corresponding repressor proteins (*tetR*, *lacI*, and

https://doi.org/10.1021/acssynbio.4c00145
ACS Synth. Biol. 2024, 13, 1851−1865

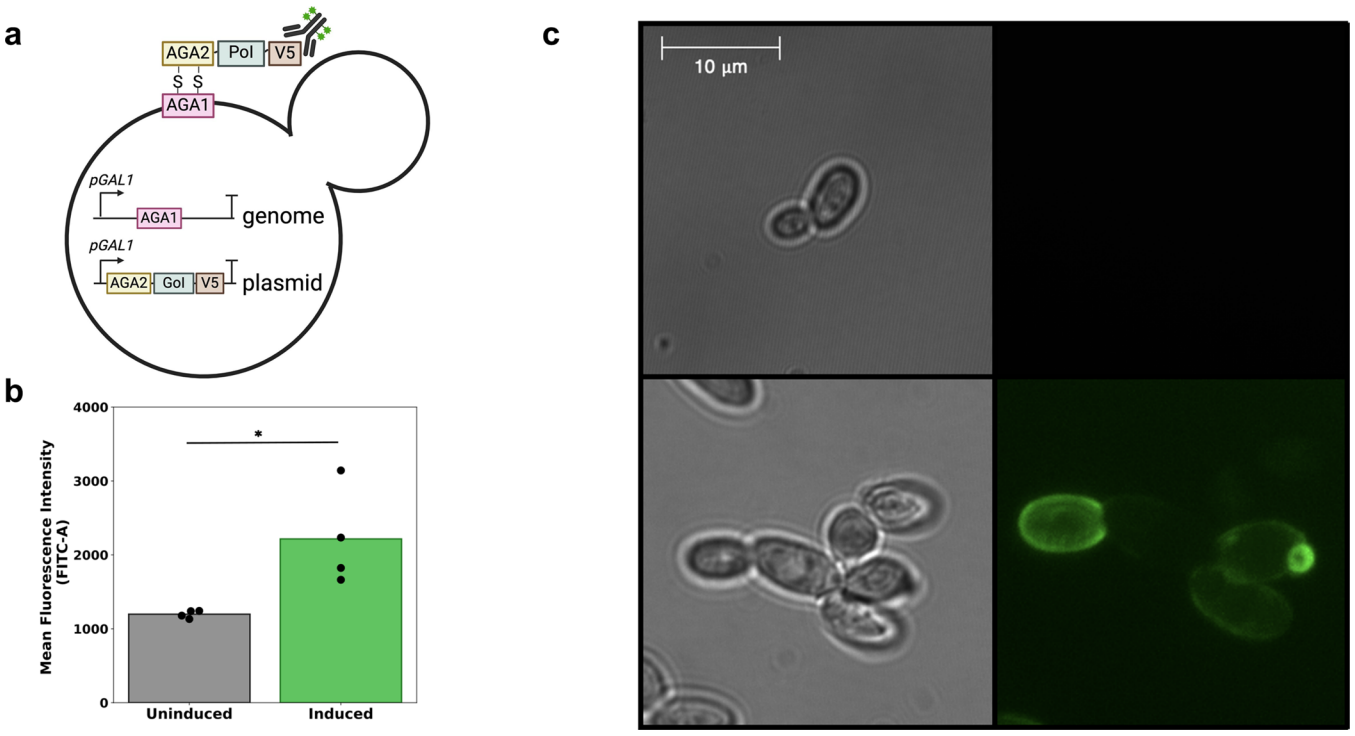

Figure 3. Inducible promoter-mediated surface display in*Sb*. (a) Schematic overview of surface display in yeast: *AGA1* is integrated into the genome, while *AGA2* and the Gene of Interest (*GoI*) are placed on a low copy number plasmid, both under the control of the *pGAL1* promoter. Upon exposure to galactose, the Protein of Interest (PoI) is expressed and anchored to the cell wall via disulfide bonds between Aga1p and Aga2p. (b) Display of SA1, a short peptide that binds to and inhibits the activity of Toxin A from *Clostridioides difficile* on the *Sb* surface. The expression levels of SA1 on the surface of *Sb* were compared between induced and noninduced conditions using immunoflow cytometry across three biological replicates. (c) Confocal microscopy images of *Sb* expressing SA1 without (top) and with (bottom) induction. Left panels show brightfield images, while right panels show fluorescence enabled by an antibody that binds to the V5 tag on SA1. Unpaired *t* test was conducted between uninduced and induced groups (* =$P <$ 0.05)

xylR, respectively) under the control of constitutive promoters. Glucose was used as the carbon source for all strains except the *pGAL1-yeGFP* strain, for which raffinose was used as a carbon source to avoid repression of *pGAL1* by glucose.

All five systems showed increasing fluorescence with increasing inducer concentration, demonstrating ligand-responsive gene expression in *Sb* (Figure 2A−E). *pCUP1* exhibited the highest maximal fluorescence, followed by *pGAL1*, *pLAC*, *pXYL*, and *pTET*. Maximal *pCUP1* expression represented 206% of *pCCW12* expression, thereby placing these promoters in the context of a previously established *Sb* promoter toolkit.[26] *pGAL1* and *pLAC* had tighter off-states, with negligible (no fluorescence above background) fluorescence detected for the lowest inducer concentrations tested (0.002% galactose and 0.5 mM IPTG). *pGAL1* had the highest fold change (245.1), followed by *pLAC* (64.7), *pTET* (44.4), *pXYL* (9.8), and *pCUP1* (3.5). The inducible systems displayed somewhat differing single-cell fluorescence distributions in response to induction, as measured by flow cytometry (Figure S2). The *pCUP*, *pGAL*, and *pTET* systems (Figure S2A−C) exhibited population distributions that shifted uniformly toward high fluorescence values as inducer concentration was increased, while the *pLAC* and *pXYL* systems displayed both increasing mean fluorescence level and increasing variability in fluorescence with increasing induction (Figure S2D,E). Notably, *pLAC* required a high concentration of IPTG to reach high expression levels, and the construct did not appear to be stable above 250 mM IPTG, as evidenced by a stark loss of fluorescence in its low-expressing subpopulation.

The *pCUP1* promoter exhibited a high fluorescence level in its uninduced condition, matching previous reports that it is a "leaky" promoter.[43] In contrast, the *pGAL1* promoter was sensitive to low concentrations of galactose, exhibiting an increase in fluorescence at less than 0.01% (w/v) galactose. While *pGAL1* does respond to galactose in *Sb*, *SbGal*$^+$ enables simultaneous growth and induction in galactose alone (Figure S3A,B) or in the presence of both galactose and raffinose (Figure S3C). Although raffinose does contain a galactose monosaccharide, raffinose alone does not significantly activate transcription from the *pGAL1* promoter in *Sb* or *SbGal*$^+$ (Figure S3C). The fold induction, sensitivity, and basal/peak expression levels we observed for these inducible systems, as well as inducer characteristics such as cost, toxicity, and stability, indicate that these inducible systems could be applicable across a wide range of application areas.

Inducible Systems Enable Tunable Gene Expression in an Anaerobic Environment. We next chose to investigate the performance of *pXYL*, *pLAC*, and *pGAL* under gut-like (i.e., anaerobic) conditions, selecting these systems due to their favorable dynamic range, low leakiness, and nontoxicity. yeGFP requires oxygen to fluoresce, so we selected the fluorescent protein CaFbFP (*Candida albicans*-adapted flavin-based fluorescent protein) for use as an anaerobic reporter of gene expression.[45,46] Flavin-based fluorescent proteins do not require oxygen to fold.[45] We placed *CaFbFP* under the control of the three inducible promoters selected, transformed these plasmids into *SbGal*$^+$ along with corresponding repressor plasmids as

https://doi.org/10.1021/acssynbio.4c00145
ACS Synth. Biol. 2024, 13, 1851−1865

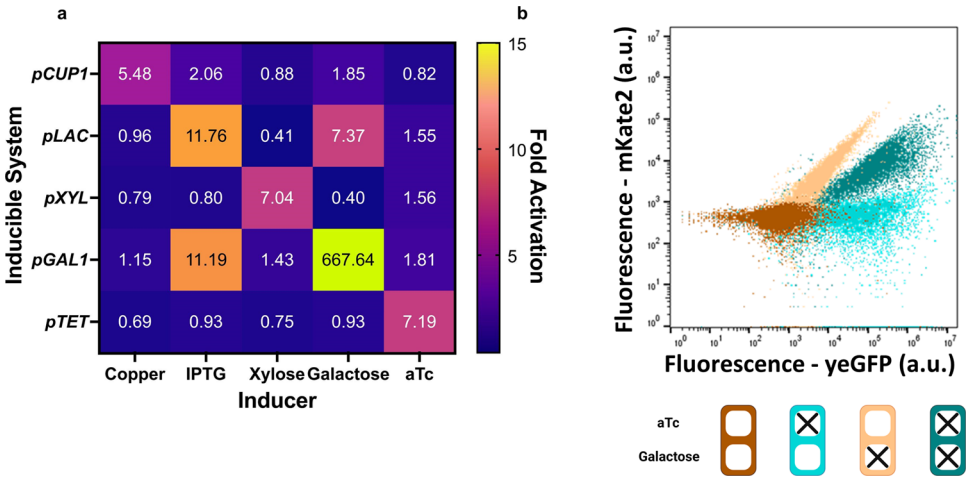

Figure 4. Orthogonality and composability of inducible promoters in (a) Evaluating the cross reactivity between the five inducible promoters driving yeGFP expression when exposed to various inducers. Each system was cultivated in CSM media lacking either only uracil or both uracil and histidine, and supplemented with 2% raffinose, in addition to a high concentration of the appropriate inducer (50 μM copper (II) sulfate, 500 mM IPTG, 40 mM xylose, 2% galactose, 1000 ng/μL anhydrotetracycline, respectively). Color intensity is represented as the average ratio of induced promoter activity to that of the reference (uninduced state). (b) Dual-fluorescence experiment demonstrating simultaneous expression of yeGFP and mKate, showcasing the potential of employing multiple inducible promoters within the same system. The orthogonal behavior of pTET and pGAL1 is evidenced by the distinct fluorescence patterns observed under different induction conditions: no inducer (brown), aTc only (light blue), galactose only (tan), and both aTc and galactose (blue-green).

necessary and cultivated the resulting strains under both aerobic and anaerobic conditions.

All three promoters demonstrated activation under anaerobic conditions (Figure S4). Interestingly, *pLAC* and *pXYL* exhibited lower maximum activation under anaerobic conditions than in aerobic conditions (maximal fluorescence decreased by 76% for *pLAC* and 78% for *pXYL*), while *pGAL1* demonstrated higher maximum activation (61% increase in maximal fluorescence). The high maximal activation of *pGAL1* in the anaerobic environment, its high dynamic range in the anaerobic environment (169×), as well as the presence of galactose as a major component of human mucins[47] makes *pGAL1* an attractive candidate for applications in the gut.

Additionally, we observed that the CaFbFP dose−response curves for *pLAC* (under both aerobic and anaerobic conditions) approached saturation with high concentrations of IPTG. This was not observed in the dose−response curve produced using yeGFP (Figure 2). The concentrations and fluorescence signals of flavin-based fluorescent proteins have previously been shown to decrease over time in *E. coli* cells growing exponentially, likely due to a depletion of flavin mononucleotide (FMN) necessary for fluorescence, as well as increased degradation of the proteins by proteases.[48] We posit that the "early" saturation we observe in CaFBFP dose−response curves is a consequence of this same mechanism. Nevertheless, this data indicates that *pLAC*, *pXYL*, and *pGAL1* are functional under the anaerobic conditions that are present in the large intestine.

Inducible Systems Enable Ligand-Responsive Surface Display in *S. boulardii*. Having demonstrated inducible gene expression in *Sb* under anaerobic conditions, we used these systems to enable cell surface display of a therapeutic peptide. Surface display of proteins on the cell surface of commensal bacteria has enabled the discovery of host-microbiome interactions and has modulated their colonization/localization within the gut.[49] Therefore, enabling surface display in *Sb* will add to its programmability as a therapeutic. In *S. cerevisiae*, surface display is often enabled by fusing the protein of interest to Aga2p.[50] Upon expression of the fusion protein, the protein of interest localizes to the cell surface through disulfide bonds that form between Aga1p and Aga2p.[51] To investigate the utility of inducible systems for enabling surface display in *Sb*, we engineered *SbGal*$^+$ to display a short peptide that binds to and inhibits the activity of Toxin A from *Clostridioides difficile* (SA1).[52] *C. difficile* infections cause colon inflammation and diarrhea and are the most frequently reported nosocomial infection in the United States.[53] The ability to inducibly display short peptides that block *C. difficile* toxin activity could enable programmable, targeted treatment and prevention of *C. difficile* infection using *Sb*.

Following the design of *S. cerevisiae* EBY100, a commonly used yeast strain for surface display, we expressed the cell surface anchor protein Aga1p in the genome via *pGAL1* and expressed an Aga2p-SA1 fusion protein with a V5 tag under inducible control of *pGAL1* on a low-copy plasmid (Figure 3A). Because surface display of recombinant proteins is often toxic, inducible expression is preferable to constitutive expression because it enables the cell population to grow to the requisite size *in vivo* before initiating surface display. To verify the display of SA1, we exposed induced and uninduced cells to an anti-V5 antibody conjugated with FITC to enable detection of displayed SA1 via flow cytometry and fluorescence microscopy. Cell cultures exposed to galactose demonstrated a significant increase in mean fluorescence compared to uninduced cultures (Figure 3B). Similarly, fluorescence microscopy of uninduced and induced samples exposed to the anti-V5 antibody demonstrated sharp localization of fluorescence to the cell wall, indicating a successful display of the SA1 peptide (Figure 3C). No fluorescence above the background was detected for uninduced samples. Immunoflow fluorescence histograms indicated that the increase in average fluorescence observed for induced samples was primarily driven by a small portion of the population that exhibits high fluorescence, consistent with previous work (Figure S5).[54] The ability of *Sb* to inducibly display proteins enhances its potential utility as an engineered biotherapeutic, although further work is necessary to determine

https://doi.org/10.1021/acssynbio.4c00145
ACS Synth. Biol. 2024, 13, 1851−1865

the absolute number of displayed proteins under various induction conditions.

Inducible Systems Enable Orthogonal Gene Expression. Engineered microbes can be programmed to make use of multiple inducible promoters, each responding to different inducers, to control the expression of multiple genes. We wished to investigate whether any inducible promoters in our library responded to inducer molecules from other systems, as such "crosstalk" could present a barrier to engineering programmable expression and more complex circuit behaviors. To check for inducer crosstalk, we grew yeast cultures harboring each inducible system in cultures containing high concentrations of each of the five inducer molecules, as well as a no-inducer control. Flow cytometry was used to check for fluorescence in each culture. We found that two inducible systems, the *pGAL1* and *pLAC* system, exhibited significant crosstalk, with galactose inducing a 7.4-fold increase in *pLAC* expression and IPTG producing a 11.2-fold increase in *pGAL1* expression (Figure 4A). This lack of orthogonality between these two systems most likely arises from the chemical similarity between IPTG and galactose. The *pGAL1* system exhibited the highest fold-change (667.6-fold) in expression following induction with the intended ligand, while *pCUP1* had the lowest fold-change (5.5-fold), followed by *pXYL* and *pTET*. This data demonstrates that although the five inducible systems are not fully orthogonal, several sets of two systems exist with minimal crosstalk between them, enabling construction of transcriptional logic gates.

To further ensure that multiple inducible systems can operate simultaneously within the same cell, we next sought to simultaneously express two different fluorescent proteins (yeGFP and mKate2) using *pTET* and *pGAL1*, which exhibited low levels of crosstalk. yeGFP and mKate2 fluoresce at different wavelengths, enabling them to be detected separately by flow cytometry. We constructed a single plasmid containing *mKate2* under the control of *pGAL1* and *yeGFP* under the control of *pTET*. *TetR*, the cognate repressor of *pTet*, was placed under constitutive control on a separate plasmid. The two plasmids were cotransformed into *SbGal*$^+$. To demonstrate simultaneous, independent activation of both inducible systems, the strain was exposed to four conditions (aTc, galactose, both inducers, and no inducers) and fluorescence of mKate2 (controlled by *pGAL1*) and yeGFP (controlled by *pTET*) was measured using flow cytometry. Figure 4B shows a representative scatterplot of the simultaneous and independent activation of two reporter proteins controlled by two inducible systems in the same cell. Because galactose-only induction showed a substantial signal in both fluorescence channels, we confirmed that mKate2 emits in both channels via constitutive expression of mKate2 alone, thereby ruling out leaky expression of GFP (Figure S6A). Other pairs of inducible systems are also capable of simultaneous orthogonal induction (e.g., *pTET* and *pCUP1* or *pTET* and *pXYL*), demonstrating that this library of systems can be used to construct more complex circuits.

Galactose Metabolism Prolongs Gut Colonization by *Sb*. Gut mucus is decorated with glycans that serve as a primary carbon source for many intestinal microbes.[55] These glycans are primarily composed of galactose, N-acetylglucosamine, N-acetylgalactosamine, fucose, and sialic acid.[56] Due to galactose's presence on intestinal mucus, we hypothesized that the ability to metabolize galactose would provide a colonization advantage to *SbGal*$^+$ over wild-type *Sb*. To test this hypothesis, we first integrated a nourseothricin resistance marker (*NatR*) to *SbGal*$^+$ and *Sb* to create strains that can grow on nourseothricin-containing selective plates (which eliminate bacterial and fungi present in fecal samples).[26] The two strains were then delivered to two different groups of antibiotic-treated mice (a total of 4 groups). Both groups of mice consumed a noncaloric sweetener sucralose in their water (S), but one of these groups of mice also consumed galactose (S + G). After three consecutive days of *Sb* administration, fecal *Sb* levels were measured every day for one week (Figure 5a). Subsequently, intestinal *Sb* levels were measured at the end of the experiment (day 9). We observed that both *Sb* and *SbGal*$^+$ attained roughly the same colonization level during the experiment, indicating that intestinal galactose is

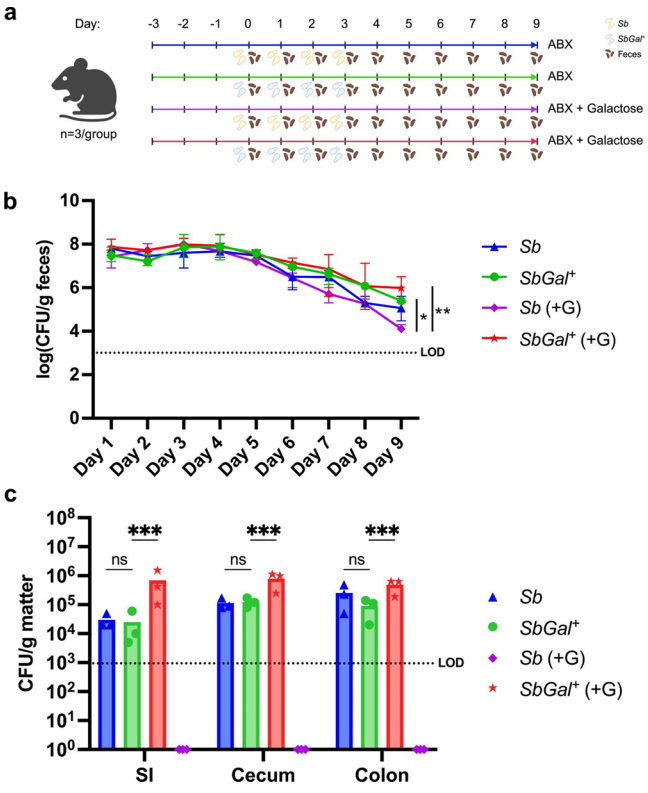

Figure 5. Modulation of *Sb* colonization profile and residence time in the mouse gut via addition of inducing sugars. (a) Schematic overview of the mice groups and timeline for antibiotics, galactose and *Sb* administration, and fecal sample collection. (b) Colonization profile of wild-type *Sb* and *SbGal*$^+$ in conventionally raised mice that were given an antibiotic cocktail (ampicillin (0.5 mg/mL), gentamicin (0.5 mg/mL), metronidazole (0.5 mg/mL), neomycin (0.5 mg/mL), vancomycin (0.25 mg/mL), and sucralose (4 mg/mL)) throughout the experiment. Galactose (2 mg/mL) was administered in water starting from Day 0. 10^8 CFUs of *SbGal*$^+$ and *Sb* were given to the mice for 4 days. Fecal samples were collected daily and plated on YPD media containing antibiotics. One-way ANOVA with Sidak's multiple comparisons test were conducted between the slopes of the regression lines for *Sb*, *SbGal*$^+$, Sb (+G), and *SbGal*$^+$ (+G) treatment groups (ns $P > 0.05$, *$P < 0.05$, **$P < 0.005$, ***$P < 0.0005$, ****$P < 0.0001$). Linear regressions were performed on log-transformed CFU/g data prior to averaging across replicates, and best fit lines are provided in Figure S7. The standard error used for ANOVA was the standard error of the slope estimate. (c) Colonization of the small intestine (SI), cecum and colon by *Sb* and *SbGal*$^+$ in this antibiotic treated mouse model. Error bars indicate the SD among the 3 mice in each experimental arm. For each gastrointestinal section data sets, two-way ANOVA with Sidak's multiple comparisons test was conducted between *Sb*, *SbGal*$^+$, Sb (+G), and *SbGal*$^+$ (+G) treatment groups (ns $P > 0.05$, * $P < 0.05$, ** $P < 0.005$, *** $P < 0.0005$).

https://doi.org/10.1021/acssynbio.4c00145
ACS Synth. Biol. 2024, 13, 1851−1865

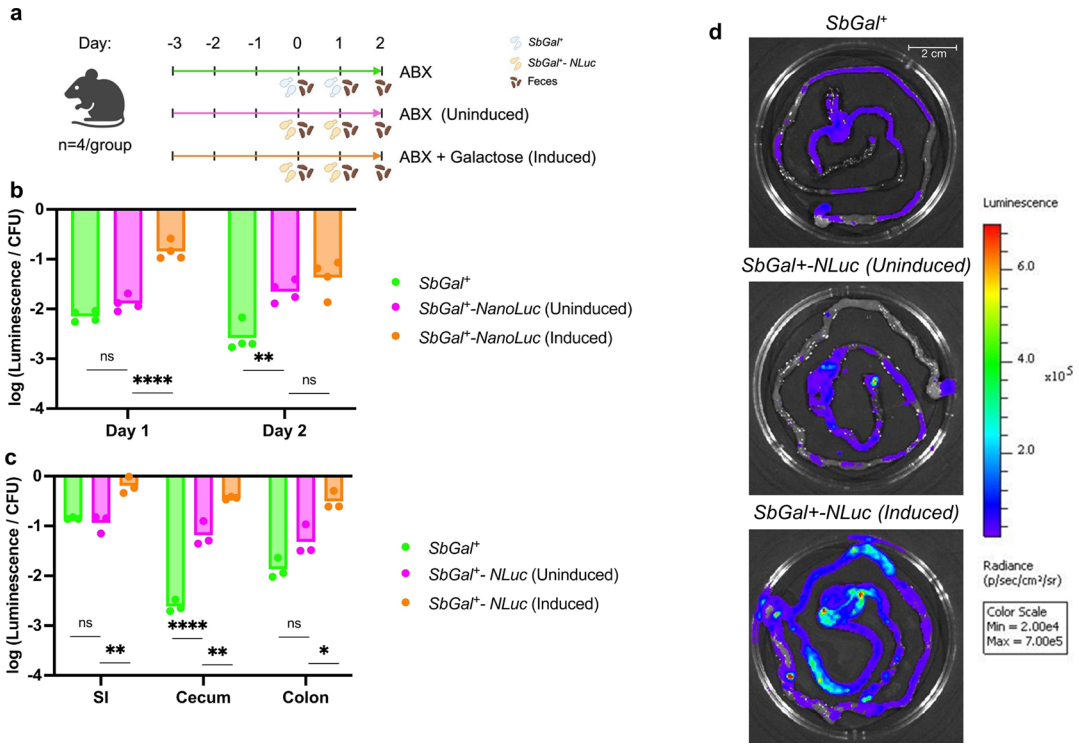

Figure 6. Inducible protein expression in the mammalian gut using *SbGal*$^+$. NanoLuciferase expressed via *pGAL1* was used to evaluate in vivo protein expression. (a) Schematic overview of the mice groups and timeline for antibiotics, galactose and *Sb* administration, and fecal sample collection. (b) Detection of NanoLuciferase in fecal matter over days of *SbGal*$^+$ and galactose treatment. (c) Localization and distribution of NanoLuciferase throughout distinct sections of the lower GI tract, including the small intestine (SI), cecum, and colon. (d) Luminescence images of NanoLuciferase activity in the GI tract, demonstrating spatially distinct expression patterns across different GI tract regions. Each dot represents one mouse in each experimental arm. For each gastrointestinal section samples and day samples, one-way ANOVA with Sidak's multiple comparisons test was conducted between *SbGal*$^+$, *SbGal*$^+$ (uninduced) and *SbGal*$^+$ (induced) treatment groups (ns $P > 0.05$, * $P < 0.05$, ** $P < 0.005$, *** $P < 0.0005$, **** $P < 0.0001$).

not sufficient to significantly enhance the colonization of *Sb*. However, upon administration of galactose, *SbGal*$^+$ maintained an increased abundance by more than 3 orders of magnitude on day 9, as compared to *Sb* (Figure 5b). To account for experimental variability introduced by the small number of mice in each group, a best-fit line was fit to logarithmically transform colonization data for each condition, enabling comparison of colonization between conditions (Figure S7). The half-life of the *Sb* population in feces over time, as measured by the slope of an exponential decay curve, was significantly higher for *SbGal*$^+$ than for *Sb* during galactose administration. This improved colonization was also reflected in the CFU measurements of intestinal contents, with *SbGal*$^+$ exhibiting higher levels of colonization of the small intestine, cecum, and colon, as compared to *Sb* during galactose administration (Figure 5c). Additionally, during galactose administration, *SbGal*$^+$ was recovered from the small intestine at levels comparable to the cecum and colon, in contrast to *Sb*, which was absent from all sampled locations on day 9 of galactose administration. These findings agree with those of Liu et al., which showed that galactose is toxic to wild-type *Sb*.[41] Small intestinal colonization unveils expanded opportunities for disease treatment beyond those specific to the large intestine, including nutrient provision to the human host. The ability to tune the abundance of *SbGal*$^+$ using galactose promises enhanced bioavailability and dosage control of delivered therapeutics.

Inducible Systems Enable On-Demand Protein Production in Mouse Models. To determine whether the *pGAL1* promoter can be employed to inducibly produce recombinant proteins in the mouse gut using *Sb*, we integrated nanoluciferase (*NanoLuc*) under the control of the *pGAL1* promoter into Site 5 of the *SbGal*$^+$ genome to produce the strain *SbGal*$^+$*NanoLuc*.[26] Nanoluciferase is a small ATP-independent luciferase that produces a luminescent signal upon exposure to furimazine or its derivatives.[57] We first found that *SbGal*$^+$*NanoLuc* was able to inducibly produce NanoLuc when cultured in synthetic media (CSM-URA), with maximum luminescence signal detected, in the cultures, 5 min after the addition of substrate to the sample (Figure S8A,B). Prior to investigating the behavior of this system in the mouse gut, we investigated how mouse chow would affect *pGAL1* induction, under the suspicion that inducing sugars might be present. We cultured *SbGal*$^+$ expressing yeGFP from *pGAL1* in a mouse chow diet-derived medium with and without additional galactose. While some activation of *pGAL1* was observed in the chow diet without galactose, yeGFP fluorescence was 15.5-fold higher when the chow diet was supplemented with galactose, demonstrating that inducible activation of *pGAL1* is possible within the chow diet media (Figure S8C).

Next, we sought to induce the production of NanoLuc *in vivo* in the mouse gut using *pGAL1*. We exposed three groups of antibiotic-treated mice ($n = 4$) to various *Sb* strains and sugars (in water) over the course of two days (Day 0 – Day 1) (Figure 6A). The first group of mice received *SbGal*$^+$ and the noncaloric sweetener sucralose in their water to serve as a control group and provide background luminescence measurements. The remaining two groups both received *SbGal*$^+$*NanoLuc*. One group

https://doi.org/10.1021/acssynbio.4c00145
ACS Synth. Biol. 2024, 13, 1851−1865

received sucralose in their water, while the other received both sucralose and galactose as an inducer. Fecal samples were collected daily for two days and NanoLuc luminescence was measured. After two days, mouse intestinal tissues were collected for CFU count assays, NanoLuc activity assays, and imaging of NanoLuc luminescence. To minimize the unequal distribution of the Nano-Glo substrate (a furimazine derivative) due to peristalsis, whole intestines were immersed for 5 min in a Nano-Glo solution prior to imaging. All luminescence values were normalized by CFU, as determined by the plating of intestinal contents.

Fecal samples from mice treated with the *SbGal*$^+$*NanoLuc* and galactose exhibited higher luminescence on Day 1 of the experiment than samples from mice treated with *SbGal*$^+$*NanoLuc* but no galactose, demonstrating effective induction of NanoLuc production in the gut via galactose (Figure 6B). Although the increased luminescence of the induced condition compared to the induced condition was not significant on Day 2, bulk luminescence of intestinal contents extracted on Day 2, normalized by CFU counts for extracted material, showed a significantly higher luminescence for the induced *SbGal*$^+$*NanoLuc* condition compared to the uninduced *SbGal*$^+$*NanoLuc* condition and *SbGal*$^+$ control condition for all three locations tested (small intestine, cecum, and colon) (Figure 6C). The nonsignificant results obtained for Day 2 fecal material may have occurred because gavaging of yeast stopped after Day 1 of the experiment. The high per-cell luminescence values observed in the *SbGal*$^+$ control condition for the small intestine (relative to the cecum and colon) are due to low colonization levels, as the raw luminescence levels were similar across the intestinal groups (data not shown).

"Leaky" expression of NanoLuc in the uninduced condition relative to the *SbGal*$^+$ control condition appeared to be particularly high in the cecum. Bioluminescence imaging of tissue samples extracted on Day 2 confirmed that the small intestine and cecum exhibited the highest accumulation of NanoLuc upon galactose induction, followed by the colon (Figure 6D). Because whole tissues were immersed in Nano-Glo substrate prior to imaging, we expect that the spatial patterns in luminescence faithfully reflect *SbGal*$^+$ abundance within the intestines, as "per-cell" luminescence was relatively constant across the gut in the induced condition (Figure 6C). These data show the spatial distribution of probiotic yeast in the gut at the millimeter scale and indicate that *pGAL1* enables inducible control of recombinant protein production in the mouse gut. This observation, combined with the fact that the uninduced *SbGal*$^+$*NanoLuc* condition enabled significantly higher luminescence than the *SbGal*$^+$-only control on both days suggests that galactose present in the gut mucus and mouse diet is sufficient for some degree of activation of *pGAL1*, but that this basal level of activation can be enhanced through supplementation of additional galactose.

Inducible Systems Enable In Vivo Logical Operations in the Mouse Gut. We next sought to demonstrate in vivo programmable gene expression in *Sb* by constructing logic gates using two of these inducible systems. We chose aTc and galactose due to their low degree of crosstalk, nontoxicity, and previous use of aTc for activating transcription in the mammalian gut.[58,59] Additionally, the presence of galactose within the gut mucus may serve to restrict engineered gene expression to the gut, thus promoting biocontainment. We constructed a transcriptional AND gate in which both galactose and aTc are necessary for activation of transcription, by cloning two Tet operators (separated by a T-rich spacer) downstream of the *pGAL1* promoter, which contains an operator for the Gal4p activator. The spacer separates the operators to prevent steric competition between repressor and activator proteins, and the high T content facilitates nucleosome depletion, enabling polymerase access to the promoter region.[44] In the absence of aTc, the TetR repressor is bound to the Tet operator sites, preventing readthrough, while in the absence of galactose, the Gal4p activator is absent, preventing transcription. Only when both inducers are present should transcription of downstream genes occur. Nanoluciferase (NanoLuc) was selected as the reporter for *pGalTet* activity. A plasmid containing the AND-gate NanoLuc unit was transformed to *SbGal*$^+$ along with a second plasmid encoding the corresponding TetR repressor to produce the strain *SbGal*$^+$*AND*.

We first tested the behavior of the *pTET* promoter alone as well as the *pGalTet* transcriptional logic gate in vitro in both synthetic media and in mouse chow media. We found that *pTET* is functional in chow media, although the maximum fluorescence signal obtained from a *pTET-yeGFP* reporter was lower in chow media than in synthetic media (Figure S9A). Having demonstrated *pTET* functionality in chow media, we next examined the behavior of the *pGalTet* transcriptional logic gate driving the production of NanoLuc in synthetic media. We found high NanoLuc production when both inducers are present compared to lower production when only galactose is present, and no luminescence above the background was observed under the "aTc only" and "no inducer" conditions (Figure S9B). This behavior demonstrates that *pGalTet* is not a perfect AND gate, as some transcriptional activation occurs in the presence of galactose alone. Nevertheless, this in vitro characterization indicated that *SbGal*$^+$*AND* would function predictably for in vivo experiments.

To examine the logical behavior of *SbGal*$^+$*AND* in the mammalian gut, four groups of antibiotic-treated mice (n = 4) were treated with *SbGal*$^+$*AND* for 3 days (Figure 7A). Starting on Day 0, each group of mice received either no inducer, galactose only, aTc only, or both galactose and aTc in their water. As before, fecal samples were collected daily for two days, after which samples of GI contents were taken. Fecal samples from mice exposed to at least one inducer demonstrated significantly higher NanoLuc production than mice exposed to no inducers, confirming that the logic gate does not exhibit pure *AND* behavior (Figure 7B). However, when mice were treated with both inducers, we observed a more significant increase in luminescence. Additional engineering would be required to achieve tighter control over induction and a more immediate response to induction in the gut environment. A similar relationship between induction condition and luminescence was observed for cells retrieved from the mouse GI tract (Figure 7C). The synergistic interaction of both galactose and aTc was pronounced, with the luminescent output in the dual-inducer condition exceeding the cumulative effects of individual inducers. This experiment highlights the successful in vivo use of the AND gate logic system in probiotic yeast.

CONCLUSIONS

Unlike nonliving therapeutics, engineered live biotherapeutics are subject to ecological forces that impact their abundance and product expression level after administration. Because the taxonomic and metabolomic composition of the gut can vary substantially between individuals, a lack of external control of recombinant gene expression and available nutrients can

https://doi.org/10.1021/acssynbio.4c00145
ACS Synth. Biol. 2024, 13, 1851−1865

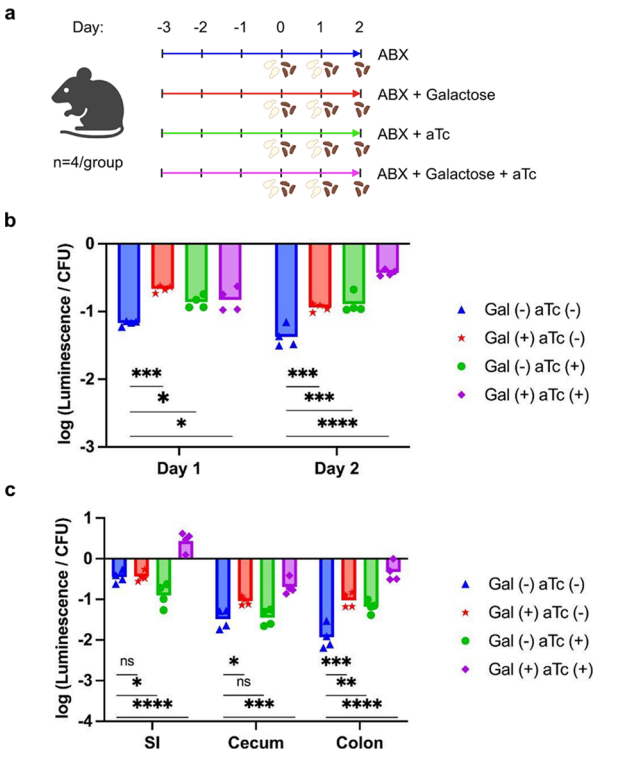

Figure 7. Development and validation of genetic logic gates for precision control of protein expression in the gut. (a) Schematic overview of the mouse groups and timeline for antibiotics, inducer and *Sb* administration, and fecal sample collection. (b) Comparative evaluation of NanoLuciferase activity under these four conditions in the mouse gut over two days, showing the functionality of the genetic logic gate in vivo. (c) NanoLuciferase expression across distinct sections of the lower GI tract, including the small intestine (SI), cecum, and colon, signifying the functionality of this gate throughout the gut. For each gastrointestinal section samples and day samples, one-way ANOVA with Sidak's multiple comparisons test was conducted between SbGal+, SbGal+ (uninduced) and SbGal+ (induced) treatment groups (ns $P > 0.05$, * $P < 0.05$, ** $P < 0.005$, *** $P < 0.0005$, **** $P < 0.0001$).

negatively impact the efficacy and safety of probiotic therapies. Here, we show that several inducible gene expression systems that are sensitive to nontoxic small molecules are suitable for controlled gene expression within *S. boulardii* and that at least two of these (*pGAL1* and galactose, *pTET,* and anhydrotetracycline) are functional in an antibiotic-treated mammalian host. As an example, we showed an inducible surface display of a toxin-binding peptide (SA1) for potential applications in sequestering bacterial toxins. In this way, the innate antibiotic resistance of *Sb* makes it ideal for use in treating bacterial infections. However, we can also envision the secretion of immunomodulators, peptide hormones, modulators of host metabolism, and bacteria-killing proteins. This inducible construct also allowed us to visualize the local biodistribution of *S. boulardii* within the intestines after antibiotic treatment. Further work is necessary to determine whether observed patterns in *Sb* abundance are due to Nano-Glo substrate diffusivity, are persistent in the face of intestinal peristalsis, and/or remain even when antibiotics are not administered. This galactose-enhanced colonization invites further exploration into the modulation of probiotic metabolism to exploit host-provided nutrients.

We also observed a low level of *pGAL1* activation in vivo, even without the addition of galactose. We rationalize this observation based on the known presence of galactose within mucus polysaccharides, as well as the presence of gut bacteria (which are known to be present in all antibiotic-treated mouse models) which may liberate galactose monosaccharides from the mucus. A testable hypothesis based on this observation is that *pGAL1* would exhibit reduced leaky expression in mono-colonized mice, or in mice without mucus-degrading bacteria.

We showed that several of these inducible systems are composable into higher-order logical functions, such as AND, thus enabling even more control over in situ therapeutic biomanufacturing. We envision that these systems could be used to activate therapeutic production (via coadministration of inducer) at the onset of treatment, followed by cessation of inducer once symptoms have resolved, thereby providing tighter control over drug dose than provided by intestinal washout alone. However, the time scale of protein induction in vivo remains to be measured and potentially shortened. Additionally, as the cost of IPTG and aTc required for maximal induction is on the order of several thousand dollars per liter of gut volume, it would be desirable to increase the sensitivity of their corresponding inducible systems. However, the relatively low mass concentration required for maximal aTc induction (500 mg/L) compared to IPTG (~60 g/L) makes aTc desirable from the perspective of patient comfort. Looking forward, we expect that the use of inducible systems with very low "off" states, coupled with biosensors that can recognize therapeutically relevant biomarkers,[60] will enable tightly controlled, autonomous disease treatment using engineered live biotherapeutics.

Serendipitously, we found that expanding *S. boulardii*'s galactose metabolism, which was necessary to enable simultaneous growth and gene expression, also conferred a colonization advantage in the mouse gut during inducer administration. While *pGAL1* seemed to be slightly activated during gut passage in the absence of additional galactose, the high sensitivity of *pGAL1* implies that naturally bioavailable galactose within the intestines is insufficient to provide a meaningful colonization advantage to *SbGal*$^+$. However, further experiments are necessary to determine whether this effect is reproducible in mice that have not been treated with antibiotics, and in more human-like gut models, because in those settings, there may exist bacteria that can more effectively compete with *Sb* for exogenous galactose. Taken together, these results imply that galactose can provide a significant level of control over the gut residence times of both *SbGal*$^+$ (which can utilize galactose as a carbon source) and *Sb* (for which galactose is toxic) in antibiotic-treated mice.

Taken together, the incorporation and in vivo functionality of inducible gene expression systems enable precision control over the dosage that *Sb* provides, as well as the location within the gut where the dose is administered. In tandem with *Sb's* capability for synthesizing small molecules, secreting proteins, or displaying proteins on its cell surface, tunable gene expression advances *S. boulardii*'s utility for therapeutic applications and studies of host-microbiome interactions.

MATERIALS AND METHODS

Strains and Culture Media. *Escherichia coli* NEB Stable, NEB 5α, and NEB 10β were used for plasmid construction and maintenance. *E. coli* cells were grown in lysogeny broth (LB) (5 g/L yeast extract, 10 g/L tryptone, 10 g/L NaCl) (at 37 °C, 250 rpm) supplemented with ampicillin (100 μg/mL), kanamycin (50 μg/mL) or chloramphenicol (34 μg/mL). *Saccharomyces boulardii* ATCC-MYA796Δ*URA3*Δ*HIS3* was used to construct *SbGal*$^+$, and *SbGal*$^+$ was used for subsequent inducible promoter characterization, yeast surface display, and logic gate experi-

https://doi.org/10.1021/acssynbio.4c00145
ACS Synth. Biol. 2024, 13, 1851−1865

ments. *Sb* strain ATCC-MYA797 was used as a control for growth characterization experiments. *Saccharomyces cerevisiae* strain BY4741 was the source for the *PGM2* gene and was used as a control for growth characterization experiments. Yeast cultures for genome editing were grown in yeast extract-peptone-dextrose (YPD) medium (50 g/L YPD Broth (Sigma-Aldrich)). For all other experiments, yeast cultures were grown in synthetic complete media containing 0.67% (w/v) yeast nitrogen base without amino acids (Sigma-Aldrich), 1.92 g/L Yeast Synthetic Media Dropout Mix (uracil, histidine, or both), and glucose (2% (w/v)) or raffinose (2% (w/v)) as a carbon source unless otherwise indicated. All *Sb* strains were grown at 37 °C and 250 rpm and all *S. cerevisiae* strains were grown at 30 °C and 250 rpm. Anaerobic cultivations were carried out in an anaerobic chamber (Coy lab, gas mix 90% nitrogen, 5% carbon dioxide, 5% hydrogen) at 37 °C with agitation at 900 rpm provided by BioShake iQ.

Plasmid and Strain Construction. A list of the strains, gene fragments, and primers used to collect the data presented in this work is shown in the Supporting Information Appendix,Tables S1−S3, while detailed sequences and maps are presented in the Supporting Information Appendix,Figures S10, S11, and Data set S1. *SbGal*$^{+}$ was constructed by replacing the *Sb PGM2* gene with the *S. cerevisiae* version via CRISPR-Cas9 genome editing. Plasmid ISA1041 provided guide RNA and Cas9 nuclease to carry the edit. A 300 bp fragment of *S. cerevisiae* PGM2 gene containing the position to be corrected was amplified via PCR and cotransformed with ISA1041 to wild-type *Sb* as described below. The selection was performed by growing transformants in synthetic media containing galactose as the sole carbon source. Editing of *PGM2* was confirmed by Sanger Sequencing.

A synthetic toolkit (MoClo-YTK) containing yeast parts was a gift from the Dueber Lab (Addgene #1000000061). Expression vectors for *yeGFP*, *mKate*, and *CaFbFP*, assembled via Golden Gate Assembly, consisted of two connectors, an inducible or constitutive promoter, the fluorescent protein coding sequence, the *tENO1* terminator, the *URA3* yeast marker, the 2 μ yeast origin, and *AmpR/ColE1* as an *E. coli* marker and origin. Similarly, expression vectors for cognate repressor proteins included two connectors, the constitutive promoter *pFBAI*,[41] the repressor protein coding sequence, the *tENO2* terminator, the *HIS3* yeast marker, the *CEN* yeast origin, and *AmpR/ColE1* as an *E. coli* marker and origin. All yeast parts were included in the MoClo-YKT kit except for the following parts, which were ordered as gBlocks from Integrated DNA Technologies, Inc. (IDT) with appropriate type-2 restriction sites and overhangs for Golden Gate Assembly: *pFBAI, tetR, lacI, xylR, CaFbFP,* and *mKate2.* The following parts were ordered as plasmids from IDT (Gene Synthesis): *pTET, pLAC, pXYL.* Expression vectors were assembled according to Deuber lab YTK protocols via Golden Gate cloning, with the Golden Gate reaction mixture containing 0.5 μL of 40 nM of each DNA part (20 fmol), 0.5 μL T7 ligase (NEB), 1.0 μL T4 Ligase Buffer (NEB), and 0.5 μL BsaI (10,000 U/mL, NEB), with water to bring the final volume to 10 μL. Assembly was performed on a thermocycler using the following program: 30 cycles of digestion (37 °C for 2 min) and ligation (16 °C for 5 min), followed by final digestion (60 °C for 10 min) and heat inactivation (80 °C for 10 min).

To construct condensed plasmids for orthogonality experiments, Gibson assembly was used to assemble both the inducible promoter-fluorescent protein transcriptional unit and constitutive promoter-cognate repressor transcriptional unit into the same backbone, separated by a connector. For each condensed plasmid, three fragments were amplified, consisting of the two transcriptional units and yeast backbone with *E. coli* marker and origin, with ∼20 bp homology between fragments. The Gibson Assembly mixture consisted of the following: 100 ng backbone fragment, additional insert fragments in 2:1 molar ratio to backbone fragment, 10 μL HiFi 2X Master Mix (NEB), and water up to 20 μL. The reactions were incubated in a thermocycler at 50 °C for 30 min prior to transformation to *E. coli*.

The pYD1 plasmid was a gift from the Wittrup Lab (Addgene #73447) and the *TRP1* marker on pYD1 was swapped with the *HIS3* marker from MoClo-YTK via 2-part Gibson cloning, resulting in DD580. Then, SA1 was ordered as primers and was inserted into MCS on DD580 via Q5 mutagenesis (DD608).

The pGAL1-AGA1-URA3 integration cassette (DD579) was constructed via Golden Gate assembly with the ISA086 backbone. AGA1 was amplified from the *Sb* genome and pGAL1 and tENO1 were amplified from the YTK.

The nourseothricin resistance gene *natR* was obtained from pYTK078 and assembled into an integration cassette (ISA186) by Golden Gate assembly as described above. The resulting integration cassette provided the DNA repair template and was transformed with CRISPR-Cas9 and gRNA targeting integration site 1[26] (ISA1045) for CRISPR-based insertion of *natR* into the *Sb* MYA 796 ΔURA ΔHIS and *SbGal*$^{+}$ genomes, producing Sb*::NatR* and *SbGal*$^{+}$*::NatR,* respectively. Transformation reactions were plated in YPD supplemented with nourseothricin and positive integrations were screened via Sanger sequencing.

Integration cassettes for logic gate constructs were constructed via Golden Gate assembly of the following parts: the integration cassette backbone, the logic gate, NanoLuc, and a transcriptional terminator. The pGalTet logic gate and the NanoLuc gene were both ordered as gBlocks with BsaI overhangs. The resulting integration cassette provided the DNA repair template and was transformed with CRISPR-Cas9 and gRNA targeting integration site 5[26] for CRISPR-based insertion of *natR* into the *Sb* MYA 796 ΔURA ΔHIS and *SbGal*$^{+}$ genomes.

Yeast Competent Cells and Transformations. We used the yeast competent cell preparation and transformation protocol from Durmusoglu et al.,[26] which is based on the protocol from Gietz et al.[60,61] To prepare competent cells, yeast colonies were inoculated into 1 mL YPD and incubated in a shaking incubator overnight at 37 °C, 250 rpm. This culture was diluted into fresh 25 mL YPD (with OD600 ≅ 0.25) and grown to OD 0.8−1.0. Cells were pelleted by centrifugation for 5 min at 3000*g* and resuspended in 25 mL autoclaved water before being centrifuged again under the same conditions. The cells were then resuspended in 1 mL lithium acetate (100 mM, Sigma-Aldrich) and centrifuged again under the same conditions. The cells were resuspended in 250 μL lithium acetate (100 mM) and divided into transformation tubes, with 50 μL/tube. Cells were washed again in 1 mL lithium acetate (100 mM) before being spun down and the supernatant removed. The cell pellet was then gently resuspended in 50 μL boiled salmon sperm DNA (2 mg/mL), and transformation reagents were added in the following order: 2 μg DNA repair template if applicable, 1 μg of any yeast plasmids (either for expression or for gRNA and Cas12a expression), 36 μL lithium acetate (1.0 M), and 260 μL PEG3350 (50%, Fisher Scientific). To produce the salmon sperm DNA, double-stranded salmon sperm DNA (Invitrogen, 15632011) at 10 mg/mL was diluted to 2 mg/mL and incubated

https://doi.org/10.1021/acssynbio.4c00145
ACS Synth. Biol. 2024, 13, 1851−1865

at 95 °C for 5 min to denature the DNA. The transformation mix was gently vortexed for less than 5 s at low speed before being heat shocked at 42 °C for one hour. The transformation reactions were then centrifuged for 3 min at 3000*g*, and the supernatant was removed and discarded. The cells were resuspended in 1 mL YPD by gentle pipetting and recovered for 1 h at 37 °C, 250 rpm (or 30 °C for *S. cerevisiae*). In the case of genome editing reactions, this recovery period was extended to a total of 3 h. Finally, the cell suspension was centrifuged for 1 min at 3000*g* and the pellet was resuspended in 100 μL. 50 μL of the suspension was plated on appropriate growth media.

***S. boulardii* Colony PCR.** Yeast genome edits were confirmed using Phire Plant Direct PCR Master Mix from Thermo Fisher. The protocol for performing PCR amplification directly from yeast colonies is described by the manufacturer. Briefly, 10 μL of the master mix was combined with 1 μL of each primer and water up to 20 μL. Using a pipet tip, a small part of a yeast colony was picked and resuspended in the PCR reaction. If the PCR failed, a modified protocol was used, as follows. A small colony was resuspended in 8 μL of 20 mM NaOH and incubated at 98 °C for 10 min. Then 10 μL of PCR master mix was added to the lysed cells, combined with 1 μL of each primer. The PCR reaction then proceeded according to the supplier's specifications. Primers were designed to bind outside the linear repair template's homology arms.

Construction of Growth Curves. Three biological replicates of each strain were grown overnight at 30 or 37 °C, 250 rpm in their corresponding media. The cultures were then subinoculated to OD 0.1 in 96-well plates (Costar, Corning 3788) in appropriate media (single and combination carbon sources) and grown for 36 h in a plate reader (BioTek Synergy H1, Shake Mode: Double Orbital, Orbital Frequency: continuous shake 365 rpm, Interval: 10 min).

Flow Cytometry Experiments. *Dose−Response Curve Construction.* Yeast strains were inoculated from single colonies on plates into 1 mL of appropriate media and grown overnight at 37 °C, 250 rpm. Cultures were then subinoculated to OD 0.1 in media containing any appropriate inducer molecules. Cultures were induced for 24 h and incubated at 4 °C for 1−2 h to facilitate protein folding (anaerobic cultures were not incubated at 4 °C). Anaerobic cultures were incubated in the anaerobic chamber. The *pCUP1*-yeGFP strain was induced in sulfate-free media to reduce nonspecific induction. The *pGAL1-yeGFP* strain was induced in media with raffinose as the carbon source to eliminate repression of promoter activity glucose. Both aerobic and anaerobic cultures were then diluted to OD 0.1−0.5 in flat-bottom 96-well plates and run on a BD Accuri C6 Plus flow cytometer. For each replicate, 10,000 events were collected under settings of FSCH-H < 20,000 and SSC-H < 600 and medium to low flow (500−2000 events/s). Fluorescence was detected on the FITC channel for yeGFP and CaFbFP. No gating was performed. Analysis was performed in FlowJo and FlowCal.[62]

Orthogonality. Yeast strains were inoculated from single colonies on plates into 1 mL of appropriate media and grown overnight at 37 °C, 250 rpm. Cultures were then subinoculated to OD 0.1 in 96-well deep well plate wells with media containing each of the inducer molecules at their highest concentration. Cultures were induced for 24 h and incubated at 4 °C for 1−2 h to facilitate protein folding. Cultures were then diluted to OD 0.1−0.5 in flat-bottom 96-well plates and run on a BD Accuri C6 Plus flow cytometer. For each replicate, 10,000 events were collected under settings of FSCH-H < 20,000 and SSC-H < 600 and medium to low flow (500−2000 events/s). yeGFP fluorescence was detected on the FITC channel and mKate2 fluorescence was detected on the PerCP channel. No gating was performed. Analysis was performed in FlowJo.

Induced Surface Display Detection. Yeast strains were inoculated from single colonies on plates into 1 mL of CSM-U media and grown overnight at 37 °C, 250 rpm. Cells were subinoculated to OD 0.5 in 5 mL CSM-U media with 1.8% galactose and 0.2% glucose and cultured for 16 h at 30 °C to induce the surface display of peptide. Five × 10^6 cells were processed for flow cytometry analysis. After media removal, cells were washed in 0.1% BSA 1× PBS. Then, they were labeled with 200 μL anti-V5 Antibody, FITC (1:250) at 800 rpm rotation at 4 °C. Cells were collected and washed in 0.1% BSA 1X PBS and resuspended in 200 μL PBS and run on a BD Accuri C6 Plus flow cytometer in 96-well plate format. For each replicate, 10,000 events were collected under settings of FSCH-H < 20,000 and SSC-H < 600 and medium flow (2000 events/s). Fluorescence was detected on the FITC channel. No gating was performed. Analysis was performed in FlowJo and FlowCal.[62]

Microscopy Imaging. Yeast suspensions were prepared by pipetting 5 μL onto a glass slide. Another glass slide coverslip was placed immediately on top of the yeast suspension droplets to create a thin film for imaging and avoid evaporation while imaging. All images were acquired using an inverted Leica DMi8 microscope with a 63× oil-immersion objective (NA = 1.40) and a Hamamatsu Orca-Fusion camera with a 60 ms exposure time. Spinning disk confocal microscopy and imaging were accomplished by using an 89 North LDI-7 Laser Diode Illuminator at 470 nm at 20% power for excitation and 510 nm for emission. When conducting confocal microscopy, maximum-intensity projection images were acquired using 10 slices with a 1 μm step size. Brightfield images used a single imaging plane. Confocal and brightfield images were obtained sequentially.

Chow/Mouse Diet Experiment. 100 g of chow oval pellets (Laboratory Rodent Diet catalog #001319) were resuspended in 1 L of DI water and filtered through a 0.22 μL filter (Catalog number: 567−0020). The filtered supernatant was used to grow Sb MYA 796 ΔURA ΔHIS and *SbGal*$^+$ with or without NanoLuciferase constructs. The expression of NanoLuciferase was measured in chow diet growth media with or without 2% galactose.

Nanoluciferase Activity Detection (In Vitro). Nanoluciferase-expressing strains were inoculated in triplicates from single colonies on plates into 1 mL of complete synthetic media (CSM) lacking uracil (-URA) (for *pGAL*) or complete synthetic media (CSM) lacking uracil and histidine (-URA-HIS) (for AND-gate) and grown overnight at 37 °C, 250 rpm. Cultures were then subinoculated to OD 0.1 in 1 mL CSM-URA or CSM-URA-HIS with respective inducers (galactose only for *pGAL1,* and either galactose only, aTc only, or both inducers for *pGalTet-NanoLuc*) and grown for 24 h at 37 °C, 250 rpm. 10 μL of each culture was collected for the luciferase assay (Promega, Nano-Glo Luciferase Assay System). Cells were diluted in 90 μL media, optical densities were measured in a plate reader (BioTek Synergy H1, absorbance 600 nm) and then mixed with 100 μL NanoGlo Assay Reagent (10 μL Nano-Glo Luciferase Assay Substrate and 90 μL sterile 1× PBS) in a 96 well black opaque plate. Cells were incubated for 5 min for a luminescent reaction to take place. Luminescence was measured in a plate reader (BioTek Synergy H1, emission 420 nm). Luminescence values were normalized by OD600 values for each replicate.

https://doi.org/10.1021/acssynbio.4c00145
ACS Synth. Biol. 2024, 13, 1851−1865

Mouse Experiments. All mouse experiments were approved by the NC State University Institutional Animal Care and Use Committee (IACUC).

Sb and SbGal⁺ Experiments. Six-week-old female C57BL/6J mice were obtained from Jackson Laboratories and hosted at the NCSU Biological Resources Facility (BRF) for 3−4 days before experiments. Mice were housed in groups of three and their cages were changed before treatment with antibiotic cocktail, and sugar administration and before treatment with *Sb* or *SbGal⁺*. Groups with galactose administration were administered with galactose (20 mg/mL) *ad libitum* in filter-sterilized drinking water starting from day 0 and refreshed daily. Antibiotic administration was started 3 days prior to the yeast gavage and continued during the experiment and refreshed daily. The antibiotic cocktail consisted of ampicillin (0.5 mg/mL), gentamicin (0.5 mg/mL), metronidazole (0.5 mg/mL), neomycin (0.5 mg/mL), vancomycin (0.25 mg/mL), and sucralose (4 mg/mL). Mice were gavaged with 10^8 CFU *Sb* (*SbGal⁺* or *Sb*) every day for 4 days (D0, D1, D2, D3). Fecal samples were collected every 24 h from day 1 to day 9. On Day 9, the mice were sacrificed, and intestinal contents (small intestine, cecum, colon) were collected.

1−2 pieces of stool or intestinal matter were collected in preweighed 1.5 mL centrifuge tubes and then weighed again to determine fecal mass. Fecal matter was then resuspended in 1 mL PBS per 10 mg feces. Fecal suspensions were plated on YPD media containing 50 μg/mL nourseothricin and 0.25 mg/mL streptomycin. Plates were sealed with parafilm and incubated at 37 °C for 2−3 days.

SbGal⁺-NanoLuc Experiments. Six-week-old female C57BL/6J mice were obtained from Jackson Laboratories and hosted at the NCSU Biological Resources Facility (BRF) for 3−4 days before experiments. Mice were housed in groups of four and their cages were changed before treatment with an antibiotic cocktail and inducer administration, and before treatment with *SbGal⁺* or *SbGal⁺-NanoLuc*. Antibiotic cocktail (ampicillin (0.5 mg/mL), gentamicin (0.5 mg/mL), metronidazole (0.5 mg/mL), neomycin (0.5 mg/mL), vancomycin (0.25 mg/mL)), sucralose (4 mg/mL) was administered *ad libitum* in filter-sterilized drinking water starting from 3 days prior to *Sb* gavage and continued throughout the experiment and refreshed daily. Galactose induction (20 mg/mL) was administered via *ad libitum* in filter-sterilized drinking water starting from Day 0 and refreshed daily. Mice were gavaged with 10^8 CFU *Sb* (*SbGal⁺* or *SbGal⁺-NanoLuc*) on Day 0 and Day 1 for 2 days. Fecal samples were collected daily (Day 1 and Day 2). On Day 2, the mice were sacrificed on Day 2 and intestinal contents (small intestine, cecum, colon) were collected.

1−2 pieces of stool or intestinal matter were collected in preweighed 1.5 mL centrifuge tubes and then weighed again to determine fecal mass. Fecal matter was then resuspended in 1 mL PBS per 10 mg feces. Serial dilutions of fecal suspensions were plated on YPD media containing 50 μg/mL nourseothricin and 0.25 mg/mL streptomycin to determine CFU counts. Plates were sealed with parafilm and incubated at 37 °C for 2−3 days.

For nanoluciferase activity detection, 100 μL of fecal suspension was serially diluted (1:10, 1:100, and 1:1000) in 1× PBS and then mixed with 100 μL of the NanoGlo Assay Reagent (10 μL Nano-Glo Luciferase Assay Substrate and 90 μL sterile 1× PBS) in a 96 well black opaque plate. Suspensions were incubated for 5 min for a luminescent reaction to take place. Luminescence was measured in a plate reader (BioTek Synergy H1, emission 420 nm). Luminescence values were normalized by CFU values for each replicate.

pGalTet-NanoLuc Experiments. Six-week-old female C57BL/6J mice were obtained from Jackson Laboratories and hosted at the NCSU Biological Resources Facility (BRF) for 3−4 days before experiments. Mice were housed in groups of four and their cages were changed before treatment with an antibiotic cocktail, inducer administration, and before treatment with *SbGal⁺* with *pGalTet-NanoLuc* (AND-gate) plasmid. Antibiotic cocktail (ampicillin (0.5 mg/mL), gentamicin (0.5 mg/mL), metronidazole (0.5 mg/mL), neomycin (0.5 mg/mL), vancomycin (0.25 mg/mL)), sucralose (4 mg/mL) was administered *ad libitum* in filter-sterilized drinking water starting from 3 days prior to *Sb* gavage and continued throughout the experiment and refreshed daily. Galactose induction (20 mg/mL) and aTc induction (0.25 mg/mL) were administered via *ad libitum* in filter-sterilized drinking water starting from Day 0 and refreshed daily. Mice were gavaged with 10^8 CFU *Sb* on Day 0 and Day 1 for 2 days. Fecal samples were collected daily (Day 1 and Day 2). On Day 2, the mice were sacrificed on Day 2 and intestinal contents (small intestine, cecum, colon) were collected.

1−2 pieces of stool or intestinal matter were collected in preweighed 1.5 mL centrifuge tubes and then weighed again to determine fecal mass. Fecal matter was then resuspended in 1 mL PBS per 10 mg feces. Serial dilutions of fecal suspensions were plated on YPD media containing 50 μg/mL nourseothricin and 0.25 mg/mL streptomycin to determine CFU counts. Plates were sealed with parafilm and incubated at 37 °C for 2−3 days.

For nanoluciferase activity detection, 100 μL of fecal suspension was serially diluted (1:10, 1:100, and 1:1000) in 1X PBS then mixed with 100 μL NanoGlo Assay Reagent (10 μL Nano-Glo Luciferase Assay Substrate and 90 μL sterile 1× PBS) in a 96 well black opaque plate. Suspensions were incubated for 5 min for a luminescent reaction to take place. Luminescence was measured in a plate reader (BioTek Synergy H1, emission 420 nm). Luminescence values were normalized by CFU values for each replicate.

One set of lower gastrointestinal tract tissue per group was collected in a Petri dish and processed for tissue imaging at BRIC Small Animal Imaging Facility core facility at UNC Chapel Hill. After collection, the tissue was transferred in ice to the facility and incubated in 10 mL NanoGlo Assay Reagent (200 μL Nano-Glo Luciferase Assay Substrate and 9.8 mL sterile 1× PBS) for 5 min shaking at 50 rpm, at room temperature. After incubation, the reagent was discarded, and the tissue was imaged for bioluminescent photon emission using IVIS Spectrum (PerkinElmer Inc.) with exposure times 1−5 min. with exposure times ranging from 1 to 5 min, depending on the signal intensity.

■ ASSOCIATED CONTENT

Supporting Information

The Supporting Information is available free of charge at https://pubs.acs.org/doi/10.1021/acssynbio.4c00145.

Growth curves for *Sb* and *SbGal⁺*, fluorescence histograms of inducible *Sb* strains, simultaneous growth and induction for *Sb* and *SbGal⁺*, induction under anaerobic conditions, fluorescence histograms for surface display constructs, fluorescence scatterplots of cells expressing two fluorescent proteins, line fitting to colonization data, induction of the *pGAL1* promoter in mouse chow media, testing AND gate functionality in vitro, graphical plasmid

https://doi.org/10.1021/acssynbio.4c00145
ACS Synth. Biol. 2024, 13, 1851−1865

maps, graphical maps for all synthetic genes, and mapping of engineered strains to the figures in which they were used, gBlocks ordered, and primer sequences (PDF)

Full gene sequences for all plasmids used in this study (ZIP)

AUTHOR INFORMATION

Corresponding Author

Nathan C. Crook − *Chemical and Biomolecular Engineering, North Carolina State University, Raleigh, North Carolina 27606, United States;* orcid.org/0000-0001-6165-1972; Email: nccrook@ncsu.edu

Authors

Deniz Durmusoglu − *Chemical and Biomolecular Engineering, North Carolina State University, Raleigh, North Carolina 27606, United States;* Present Address: Department of Biotechnology and Biomedicine, Yeast Biotechnology and Fermentation, Synthetic Biology, Technical University of Denmark, Kongens Lyngby, 2800 Kgs. Lyngby, Denmark

Daniel J. Haller − *Chemical and Biomolecular Engineering, North Carolina State University, Raleigh, North Carolina 27606, United States;* Present Address: Systems, Synthetic, and Physical Biology PhD Program, Rice University, Houston, Texas 77005, United States

Ibrahim S. Al'Abri − *Chemical and Biomolecular Engineering, North Carolina State University, Raleigh, North Carolina 27606, United States*

Katie Day − *Chemical and Biomolecular Engineering, North Carolina State University, Raleigh, North Carolina 27606, United States*

Carmen Sands − *Novo Nordisk Foundation Center for Biosustainability, Technical University of Denmark, 2800 Kgs. Lyngby, Denmark*

Andrew Clark − *Chemical and Biomolecular Engineering, North Carolina State University, Raleigh, North Carolina 27606, United States*

Adriana San-Miguel − *Chemical and Biomolecular Engineering, North Carolina State University, Raleigh, North Carolina 27606, United States*

Ruben Vazquez-Uribe − *Novo Nordisk Foundation Center for Biosustainability, Technical University of Denmark, 2800 Kgs. Lyngby, Denmark*

Morten O. A. Sommer − *Novo Nordisk Foundation Center for Biosustainability, Technical University of Denmark, 2800 Kgs. Lyngby, Denmark;* orcid.org/0000-0003-4005-5674

Complete contact information is available at: https://pubs.acs.org/10.1021/acssynbio.4c00145

Author Contributions

[§]D.D., D.J.H., and I.S.A. contributed equally to this work. D.D., D.J.H., I.S.A., and N.C. designed and conceived the study. D.D., D.J.H., I.S.A., C.S., and K.D. performed all yeast engineering and cultivation experiments. D.D. led all mice experiments with help from I.S.A. A.C. and D.D. performed and analyzed microscopy imaging for yeast display. N.C. supervised the research. D.D., D.J.H., I.S.A., and N.C. wrote the manuscript. N.C., A.S.M., R.V.U., and M.O.A.S. solicited funding. All authors read and approved the final manuscript.

Notes

The authors declare the following competing financial interest(s): ISA, DD, DJH, and NC have filed a patent application related to this work.

ACKNOWLEDGMENTS

We gratefully acknowledge experimental assistance from Dr. Jonathan Frank at the BRIC Small Animal Imaging Facility core facility at UNC Chapel Hill, Sandy Elliot at the NCSU Biological resources facility, and members of the Crook lab for helpful discussions. DD and NC were supported by the National Science Foundation (CBET-1934284) and the Novo Nordisk Foundation (NNF19SA0035474). I.S.A. is supported by NCSU CBE startup funds and the Ministry of Higher Education - Oman. D.J.H. was supported by the NC State Park Scholarship. A.C. and A.S.M. were supported by the National Science Foundation (MCB-1947498). C.S., R.V.-U., and M.O.A.S. were supported by the Novo Nordisk Foundation (NNF20CC0035580, NNF17CO0028232, and NNF19SA0035438).

REFERENCES

(1) Pedrolli, D. B.; Ribeiro, N. V.; Squizato, P. N.; de Jesus, V. N.; Cozetto, D. A.; Tuma, R. B.; Gracindo, A.; Cesar, M. B.; Freire, P. J. C.; da Costa, A. F. M.; Lins, M. R. C. R.; Correa, G. G.; Cerri, M. O. Engineering Microbial Living Therapeutics: The Synthetic Biology Toolbox. *Trends in Biotechnology* **2019**, *37* (1), 100−115.

(2) Isabella, V. M.; Ha, B. N.; Castillo, M. J.; Lubkowicz, D. J.; Rowe, S. E.; Millet, Y. A.; Anderson, C. L.; Li, N.; Fisher, A. B.; West, K. A.; Reeder, P. J.; Momin, M. M.; Bergeron, C. G.; Guilmain, S. E.; Miller, P. F.; Kurtz, C. B.; Falb, D. Development of a Synthetic Live Bacterial Therapeutic for the Human Metabolic Disease Phenylketonuria. *Nat. Biotechnol.* **2018**, *36* (9), 857−864.

(3) Hwang, I. Y.; Koh, E.; Wong, A.; March, J. C.; Bentley, W. E.; Lee, Y. S.; Chang, M. W. Engineered Probiotic Escherichia Coli Can Eliminate and Prevent Pseudomonas Aeruginosa Gut Infection in Animal Models. *Nat Commun* **2017**, *8* (1), 15028.

(4) Steidler, L.; Hans, W.; Schotte, L.; Neirynck, S.; Obermeier, F.; Falk, W.; Fiers, W.; Remaut, E. Treatment of Murine Colitis by Lactococcus Lactis Secreting Interleukin-10. *Science* **2000**, *289* (5483), 1352−1355.

(5) Ozdemir, T.; Fedorec, A. J. H.; Danino, T.; Barnes, C. P. Synthetic Biology and Engineered Live Biotherapeutics: Toward Increasing System Complexity. *Cell Systems* **2018**, *7* (1), 5−16.

(6) Riglar, D. T.; Giessen, T. W.; Baym, M.; Kerns, S. J.; Niederhuber, M. J.; Bronson, R. T.; Kotula, J. W.; Gerber, G. K.; Way, J. C.; Silver, P. A. Engineered Bacteria Function in the Mammalian Gut as Long Term Live Diagnostics of Inflammation. *Nat. Biotechnol.* **2017**, *35* (7), 653−658.

(7) Daeffler, K. N.; Galley, J. D.; Sheth, R. U.; Ortiz-Velez, L. C.; Bibb, C. O.; Shroyer, N. F.; Britton, R. A.; Tabor, J. J. Engineering Bacterial Thiosulfate and Tetrathionate Sensors for Detecting Gut Inflammation. *Molecular Systems Biology* **2017**, *13* (4), 923.

(8) Scott, B. M.; Gutiérrez-Vázquez, C.; Sanmarco, L. M.; da Silva Pereira, J. A.; Li, Z.; Plasencia, A.; Hewson, P.; Cox, L. M.; O'Brien, M.; Chen, S. K.; Moraes-Vieira, P. M.; Chang, B. S. W.; Peisajovich, S. G.; Quintana, F. J. Self-Tunable Engineered Yeast Probiotics for the Treatment of Inflammatory Bowel Disease. *Nat Med* **2021**, *27* (7), 1212−1222.

(9) Sen, S.; Mansell, T. J. Yeasts as Probiotics: Mechanisms, Outcomes, and Future Potential. *Fungal Genetics and Biology* **2020**, *137*, No. 103333.

(10) Michael, S.; Keubler, L. M.; Smoczek, A.; Meier, M.; Gunzer, F.; Pöhlmann, C.; Krause-Buchholz, U.; Hedrich, H.-J.; Bleich, A. Quantitative Phenotyping of Inflammatory Bowel Disease in the IL-10-Deficient Mouse by Use of Noninvasive Magnetic Resonance Imaging. *Inflammatory Bowel Diseases* **2013**, *19* (1), 185−193.

(11) Bagherpour, G.; Ghasemi, H.; Zand, B.; Zarei, N.; Roohvand, F.; Ardakani, E. M.; Azizi, M.; Khalaj, V. Oral Administration of Recombinant Saccharomyces Boulardii Expressing Ovalbumin-CPE Fusion Protein Induces Antibody Response in Mice. *Front. Microbiol.* **2018**, *9*, 723 DOI: 10.3389/fmicb.2018.00723.
(12) Hedin, K. A.; Zhang, H.; Kruse, V.; Rees, V. E.; Bäckhed, F.; Greiner, T. U.; Vazquez-Uribe, R.; Sommer, M. O. A. Cold Exposure and Oral Delivery of GLP-1R Agonists by an Engineered Probiotic Yeast Strain Have Antiobesity Effects in Mice. *ACS Synth. Biol.* **2023**, *12*, 3433.
(13) Chen, K.; Zhu, Y.; Zhang, Y.; Hamza, T.; Yu, H.; Saint Fleur, A.; Galen, J.; Yang, Z.; Feng, H. A Probiotic Yeast-Based Immunotherapy against Clostridioides Difficile Infection. *Sci Transl Med* **2020**, *12* (567), No. eaax4905.
(14) van der Aa Kühle, A.; Jespersen, L. The Taxonomic Position of Saccharomyces Boulardii as Evaluated by Sequence Analysis of the D1/D2 Domain of 26S rDNA, the ITS1−5.8S rDNA-ITS2 Region and the Mitochondrial Cytochrome-c Oxidase II Gene. *Systematic and Applied Microbiology* **2003**, *26* (4), 564−571.
(15) Tiago, F. C. P.; Martins, F. S.; Souza, E. L. S.; Pimenta, P. F. P.; Araujo, H. R. C.; Castro, I. M.; Brandão, R. L.; Nicoli, J. R. Adhesion to the Yeast Cell Surface as a Mechanism for Trapping Pathogenic Bacteria by Saccharomyces Probiotics. *Journal of Medical Microbiology* **2012**, *61* (9), 1194−1207.
(16) Khatri, I.; Tomar, R.; Ganesan, K.; Prasad, G. S.; Subramanian, S. Complete Genome Sequence and Comparative Genomics of the Probiotic Yeast Saccharomyces Boulardii. *Sci Rep* **2017**, *7*, 371.
(17) Hudson, L. E.; McDermott, C. D.; Stewart, T. P.; Hudson, W. H.; Rios, D.; Fasken, M. B.; Corbett, A. H.; Lamb, T. J. Characterization of the Probiotic Yeast Saccharomyces Boulardii in the Healthy Mucosal Immune System. *PLoS One* **2016**, *11* (4), No. e0153351.
(18) Fietto, J. L. R.; Araújo, R. S.; Valadão, F. N.; Fietto, L. G.; Brandão, R. L.; Neves, M. J.; Gomes, F. C. O.; Nicoli, J. R.; Castro, I. M. Molecular and Physiological Comparisons between Saccharomyces Cerevisiae and Saccharomyces Boulardii. *Can. J. Microbiol.* **2004**, *50* (8), 615−621.
(19) Rodrigues, A. C. P.; Cara, D. C.; Fretez, S. H. G. G.; Cunha, F. Q.; Vieira, E. C.; Nicoli, J. R.; Vieira, L. Q. Saccharomyces Boulardii Stimulates sIgA Production and the Phagocytic System of Gnotobiotic Mice. *J. Appl. Microbiol.* **2000**, *89* (3), 404−414.
(20) Guslandi, M.; Giollo, P.; Testoni, P. A. A Pilot Trial of Saccharomyces Boulardii in Ulcerative Colitis. *Eur J Gastroenterol Hepatol* **2003**, *15* (6), 697−698.
(21) Wang, C.; Li, W.; Wang, H.; Ma, Y.; Zhao, X.; Zhang, X.; Yang, H.; Qian, J.; Li, J. Saccharomyces Boulardii Alleviates Ulcerative Colitis Carcinogenesis in Mice by Reducing TNF-α and IL-6 Levels and Functions and by Rebalancing Intestinal Microbiota. *BMC Microbiol* **2019**, *19*, 246.
(22) Billoo, A.; Memon, M.; Khaskheli, S.; Murtaza, G.; Iqbal, K.; Shekhani, M. S.; Siddiqi, A. Q. Role of a Probiotic (Saccharomyces Boulardii) in Management and Prevention of Diarrhoea. *World J Gastroenterol* **2006**, *12* (28), 4557−4560.
(23) Tung, J. M.; Dolovich, L. R.; Lee, C. H. Prevention of Clostridium Difficile Infection with Saccharomyces Boulardii: A Systematic Review. *Can J Gastroenterol* **2009**, *23* (12), 817−821.
(24) Wombwell, E.; Patterson, M. E.; Bransteitter, B.; Gillen, L. R. The Effect of Saccharomyces Boulardii Primary Prevention on Risk of Hospital-Onset Clostridioides Difficile Infection in Hospitalized Patients Administered Antibiotics Frequently Associated With C. Difficile Infection. *Clinical Infectious Diseases* **2021**, *73* (9), e2512−e2518.
(25) Hedin, K. A.; Rees, V. E.; Zhang, H.; Kruse, V.; Vazquez-Uribe, R.; Sommer, M. O. A. Effects of Broad-Spectrum Antibiotics on the Colonisation of Probiotic Yeast Saccharomyces Boulardii in the Murine Gastrointestinal Tract. *Sci Rep* **2022**, *12*, 8862.
(26) Durmusoglu, D.; Al'Abri, I. S.; Collins, S. P.; Cheng, J.; Eroglu, A.; Beisel, C. L.; Crook, N. *In Situ* Biomanufacturing of Small Molecules in the Mammalian Gut by Probiotic *Saccharomyces Boulardii*. *ACS Synth. Biol.* **2021**, *10* (5), 1039−1052.
(27) Blehaut, H.; Massot, J.; Elmer, G. W.; Levy, R. H. Disposition Kinetics of Saccharomyces Boulardii in Man and Rat. *Biopharm Drug Dispos* **1989**, *10* (4), 353−364.
(28) Jensen, E. D.; Deichmann, M.; Ma, X.; Vilandt, R. U.; Schiesaro, G.; Rojek, M. B.; Lengger, B.; Eliasson, L.; Vento, J. M.; Durmusoglu, D.; Hovmand, S. P.; Al'Abri, I.; Zhang, J.; Crook, N.; Jensen, M. K. Engineered Cell Differentiation and Sexual Reproduction in Probiotic and Mating Yeasts. *Nat Commun* **2022**, *13* (1), 6201.
(29) Durmusoglu, D.; Al'Abri, I.; Li, Z.; Islam Williams, T.; Collins, L. B.; Martínez, J. L.; Crook, N. Improving Therapeutic Protein Secretion in the Probiotic Yeast Saccharomyces Boulardii Using a Multifactorial Engineering Approach. *Microbial Cell Factories* **2023**, *22* (1), 109.
(30) Liu, J.-J.; Kong, I. I.; Zhang, G.-C.; Jayakody, L. N.; Kim, H.; Xia, P.-F.; Kwak, S.; Sung, B. H.; Sohn, J.-H.; Walukiewicz, H. E.; Rao, C. V.; Jin, Y.-S. Metabolic Engineering of Probiotic Saccharomyces Boulardii. *Appl. Environ. Microbiol.* **2016**, *82* (8), 2280−2287.
(31) Sleight, S. C.; Sauro, H. M. Visualization of Evolutionary Stability Dynamics and Competitive Fitness of Escherichia Coli Engineered with Randomized Multigene Circuits. *ACS Synth Biol* **2013**, *2* (9), 519−528.
(32) Loessner, H.; Leschner, S.; Endmann, A.; Westphal, K.; Wolf, K.; Kochruebe, K.; Miloud, T.; Altenbuchner, J.; Weiss, S. Drug-Inducible Remote Control of Gene Expression by Probiotic Escherichia Coli Nissle 1917 in Intestine, Tumor and Gall Bladder of Mice. *Microbes Infect* **2009**, *11* (14−15), 1097−1105.
(33) Danino, T.; Prindle, A.; Kwong, G. A.; Skalak, M.; Li, H.; Allen, K.; Hasty, J.; Bhatia, S. N. Programmable Probiotics for Detection of Cancer in Urine. *Sci Transl Med* **2015**, *7* (289), 289ra84.
(34) Chen, Y.; Ho, J. M. L.; Shis, D. L.; Gupta, C.; Long, J.; Wagner, D. S.; Ott, W.; Josić, K.; Bennett, M. R. Tuning the Dynamic Range of Bacterial Promoters Regulated by Ligand-Inducible Transcription Factors. *Nat Commun* **2018**, *9* (1), 64.
(35) Wang, B.; Kitney, R. I.; Joly, N.; Buck, M. Engineering Modular and Orthogonal Genetic Logic Gates for Robust Digital-like Synthetic Biology. *Nat Commun* **2011**, *2* (1), 508.
(36) Bradley, R. W.; Buck, M.; Wang, B. Recognizing and Engineering Digital-like Logic Gates and Switches in Gene Regulatory Networks. *Curr Opin Microbiol* **2016**, *33*, 74−82.
(37) Piraner, D. I.; Abedi, M. H.; Moser, B. A.; Lee-Gosselin, A.; Shapiro, M. G. Tunable Thermal Bioswitches for in Vivo Control of Microbial Therapeutics. *Nat Chem Biol* **2017**, *13* (1), 75−80.
(38) Rottinghaus, A. G.; Amrofell, M. B.; Moon, T. S. Biosensing in Smart Engineered Probiotics. *Biotechnol J* **2020**, *15* (10), No. e1900319.
(39) Da Silva, N. A.; Srikrishnan, S. Introduction and Expression of Genes for Metabolic Engineering Applications in Saccharomyces Cerevisiae. *FEMS Yeast Res* **2012**, *12* (2), 197−214.
(40) Timson, D. J. The Molecular Basis of Galactosemia — Past, Present and Future. *Gene* **2016**, *589* (2), 133−141.
(41) Liu, J.-J.; Zhang, G.-C.; Kong, I. I.; Yun, E. J.; Zheng, J.-Q.; Kweon, D.-H.; Jin, Y.-S. A Mutation in PGM2 Causing Inefficient Galactose Metabolism in the Probiotic Yeast Saccharomyces Boulardii. *Appl. Environ. Microbiol.* **2018**, *84* (10), e02858−17.
(42) Siegal, M. L. Shifting Sugars and Shifting Paradigms. *PLOS Biology* **2015**, *13* (2), No. e1002068.
(43) Lee, M. E.; DeLoache, W. C.; Cervantes, B.; Dueber, J. E. A Highly Characterized Yeast Toolkit for Modular, Multipart Assembly. *ACS Synth. Biol.* **2015**, *4* (9), 975−986.
(44) Chen, Y.; Zhang, S.; Young, E. M.; Jones, T. S.; Densmore, D.; Voigt, C. A. Genetic Circuit Design Automation for Yeast. *Nat Microbiol* **2020**, *5* (11), 1349−1360.
(45) Tielker, D.; Eichhof, I.; Jaeger, K.-E.; Ernst, J. F. Flavin Mononucleotide-Based Fluorescent Protein as an Oxygen-Independent Reporter in Candida Albicans and Saccharomyces Cerevisiae. *Eukaryot Cell* **2009**, *8* (6), 913−915.
(46) Eichhof, I.; Ernst, J. F. Oxygen-Independent FbFP: Fluorescent Sentinel and Oxygen Sensor Component in Saccharomyces Cerevisiae and Candida Albicans. *Fungal Genetics and Biology* **2016**, *92*, 14−25.
(47) Takagi, J.; Aoki, K.; Turner, B. S.; Lamont, S.; Lehoux, S.; Kavanaugh, N.; Gulati, M.; Valle Arevalo, A.; Lawrence, T. J.; Kim, C.

Y.; Bakshi, B.; Ishihara, M.; Nobile, C. J.; Cummings, R. D.; Wozniak, D. J.; Tiemeyer, M.; Hevey, R.; Ribbeck, K. Mucin O-Glycans Are Natural Inhibitors of Candida Albicans Pathogenicity. *Nat Chem Biol* **2022**, *18* (7), 762−773.
(48) Mukherjee, A.; Walker, J.; Weyant, K. B.; Schroeder, C. M. Characterization of Flavin-Based Fluorescent Proteins: An Emerging Class of Fluorescent Reporters. *PLOS ONE* **2013**, *8* (5), No. e64753.
(49) Li, S.; Sha, Z.; Wang, X.; Bu, Z.; Wang, L.; Guan, X.; Lang, X.; Wang, X. Yeast Surface Display of Escherichia Coli Enterotoxin and Its Effects of Intestinal Microflora and Mucosal Immunity. *Curr. Microbiol.* **2017**, *74* (7), 854−862.
(50) Boder, E. T.; Wittrup, K. D. Yeast Surface Display for Screening Combinatorial Polypeptide Libraries. *Nat. Biotechnol.* **1997**, *15* (6), 553−557.
(51) Mei, M.; Zhou, Y.; Peng, W.; Yu, C.; Ma, L.; Zhang, G.; Yi, L. Application of Modified Yeast Surface Display Technologies for Non-Antibody Protein Engineering. *Microbiological Research* **2017**, *196*, 118−128.
(52) Sarma, S.; Catella, C. M.; San Pedro, E. T.; Xiao, X.; Durmusoglu, D.; Menegatti, S.; Crook, N.; Magness, S. T.; Hall, C. K. Design of 8-Mer Peptides That Block Clostridioides Difficile Toxin A in Intestinal Cells. *Commun Biol* **2023**, *6* (1), 1−13.
(53) Leffler, D. A.; Lamont, J. T. Clostridium Difficile Infection. *N. Engl. J. Med.* **2015**, *372*, 1539−1548.
(54) Nguyen, H.-M.; Pham, M.-L.; Stelzer, E. M.; Plattner, E.; Grabherr, R.; Mathiesen, G.; Peterbauer, C. K.; Haltrich, D.; Nguyen, T.-H. Constitutive Expression and Cell-Surface Display of a Bacterial β-Mannanase in Lactobacillus Plantarum. *Microbial Cell Factories* **2019**, *18* (1), 76.
(55) Luis, A. S.; Hansson, G. C. Intestinal Mucus and Their Glycans: A Habitat for Thriving Microbiota. *Cell Host & Microbe* **2023**, *31* (7), 1087−1100.
(56) Schroeder, B. O. Fight Them or Feed Them: How the Intestinal Mucus Layer Manages the Gut Microbiota. *Gastroenterology Report* **2019**, *7* (1), 3−12.
(57) England, C. G.; Ehlerding, E. B.; Cai, W. NanoLuc: A Small Luciferase Is Brightening up the Field of Bioluminescence. *Bioconjug Chem* **2016**, *27* (5), 1175−1187.
(58) Rottinghaus, A. G.; Ferreiro, A.; Fishbein, S. R. S.; Dantas, G.; Moon, T. S. Genetically Stable CRISPR-Based Kill Switches for Engineered Microbes. *Nat Commun* **2022**, *13* (1), 672.
(59) Lim, B.; Zimmermann, M.; Barry, N. A.; Goodman, A. L. Engineered Regulatory Systems Modulate Gene Expression of Human Commensals in the Gut. *Cell* **2017**, *169* (3), 547−558.e15.
(60) Gietz, R. D.; Schiestl, R. H. Quick and Easy Yeast Transformation Using the LiAc/SS Carrier DNA/PEG Method. *Nat Protoc* **2007**, *2* (1), 35−37.
(61) Gietz, R. D.; Schiestl, R. H. High-Efficiency Yeast Transformation Using the LiAc/SS Carrier DNA/PEG Method. *Nat Protoc* **2007**, *2* (1), 31−34.
(62) Castillo-Hair, S. M.; Sexton, J. T.; Landry, B. P.; Olson, E. J.; Igoshin, O. A.; Tabor, J. J. FlowCal: A User-Friendly, Open Source Software Tool for Automatically Converting Flow Cytometry Data from Arbitrary to Calibrated Units. *ACS Synth. Biol.* **2016**, *5* (7), 774−780.

https://doi.org/10.1021/acssynbio.4c00145
ACS Synth. Biol. 2024, 13, 1851−1865